1-2019

Seismic Monitoring and Baseline Microseismicity in the Rome Trough, Eastern Kentucky

N. Seth Carpenter
University of Kentucky, seth.carpenter@uky.edu

Andrew S. Holcomb
University of Kentucky, asholc2@g.uky.edu

Zhenming Wang
University of Kentucky, zmwang@uky.edu

John B. Hickman
University of Kentucky, john.hickman@uky.edu

Edward W. Woolery
University of Kentucky, ewoolery@uky.edu

Kentucky Geological Survey
University of Kentucky, Lexington

Seismic Monitoring and Baseline Microseismicity in the Rome Trough, Eastern Kentucky

N. Seth Carpenter, Andrew S. Holcomb, Zhenming Wang, John B. Hickman, and Edward W. Woolery

Report of Investigations 5 doi.org/10.13023/kgs.ri05.13 Series XIII, 2019

Our Mission

The Kentucky Geological Survey is a state-supported research center and public resource within the University of Kentucky. Our mission is to support sustainable prosperity of the commonwealth, the vitality of its flagship university, and the welfare of its people. We do this by conducting research and providing unbiased information about geologic resources, environmental issues, and natural hazards affecting Kentucky.

Earth Resources—Our Common Wealth

www.uky.edu/kgs

For further information contact:
Technology Transfer Officer
Kentucky Geological Survey
228 Mining and Mineral Resources Building
University of Kentucky
Lexington, KY 40506-0107

Technical Level

General **Intermediate** **Technical**

Statement of Benefit to Kentucky

This report is about small, naturally occurring earthquakes in the Rome Trough of eastern Kentucky, where several test wells have been drilled into a potential oil and gas reservoir known as the Rogersville Shale. The research described in this report may help to determine if future earthquakes are caused by fluid injection and hydraulic fracturing related to oil and gas production, which could lead to public-safety concerns or restrictions on production.

ISSN 0075-5591

Contents

Figures

Figures (continued)

Tables

Tables
(continued)

Note on Revisions (10/9/2019)

Table 1 in the original version of this report contained erroneous cumulative injection volumes for Class II wastewater disposal wells in eastern Kentucky. Those incorrect volumes were also plotted in Figure 5. This revision contains corrected values in Table 1 and a corresponding update to Figure 5.

Seismic Monitoring and Baseline Microseismicity in the Rome Trough, Eastern Kentucky

N. Seth Carpenter, Andrew S. Holcomb, Zhenming Wang, John B. Hickman, and Edward W. Woolery

Abstract

In the central and eastern United States, felt earthquakes likely triggered by fluid injection from oil and gas production or wastewater disposal have dramatically increased in frequency since the onset of the unconventional shale gas and oil boom. In the Rome Trough of eastern Kentucky, fracture stimulations and wastewater injection are ongoing and occur near areas of historical seismic activity. Unlike in surrounding and nearby states (Ohio, West Virginia, and Arkansas), in Kentucky, no seismic events related to subsurface fluid injections have been reported as felt or detected by regional seismic networks, including the Kentucky Seismic and Strong-Motion Network.

Oil and gas development of the deep Cambrian Rogersville Shale in the Rome Trough is in a very early stage, and will require horizontal drilling and high-volume hydraulic fracturing. To characterize natural seismicity rates and the conditions that might lead to induced or triggered events, the Kentucky Geological Survey is conducting a collaborative study, the Eastern Kentucky Microseismic Monitoring Project, prior to large-scale oil and gas production and wastewater injection. A temporary network of broadband seismographs was deployed near dense clusters of Class II wastewater-injection wells and near the locations of new, deep oil and gas test wells in eastern Kentucky. Network installation began in mid-2015 and by November 2015, 12 stations were operating, with data acquired in real time and jointly with regional network data. Additional stations were installed between June 2016 and October 2017 in targeted locations. The network improved the monitoring sensitivity near wastewater-injection wells and deep oil and gas test wells by approximately an entire unit of magnitude: With the temporary network, the detectable magnitudes range from 0.7 to 1.0, and without it, the detectable magnitudes range from 1.5 to 1.9.

Using the real-time recordings of this network in tandem with the recordings of other temporary and permanent regional seismic stations, we generated a catalog of local seismicity and developed a calibrated magnitude scale. At the time this report was prepared, 151 earthquakes had been detected and located, 38 of which were in the project area, defined as the region bounded by 37.1°N to 38.7°N latitude and 84.5°W to 82.0°W longitude. Only six earthquakes occurred in the Rome Trough of eastern Kentucky, none of which were reported in regional monitoring agency catalogs, and none of which appear to be associated with the deep Rogersville Shale test wells that were completed during the time the network was in operation or with wastewater-injection wells.

Introduction

Earthquakes can result from natural causes, including the sudden release of tectonic strain through earthquake cycles and from volcanic activity. They can also be caused by manmade activities such as the injection of fluids into deep boreholes. Most seismic events triggered or induced by human activity produce very low-level shaking (Ellsworth, 2013); however, some instances of wastewater injection have reactivated faults and caused felt earthquakes, some of which were large enough to cause structural damage in local communities (Taylor and others, 2017).

Since approximately 2009, the rate of felt earthquakes in the central United States has increased dramatically (Fig. 1). This increased rate has a strong correlation in space and time with the increase in production of oil and gas, and resultant subsurface disposal of produced water (Weingarten and others, 2015; Langenbruch and Zoback, 2016). The principal cause of these events has been assigned to the injection of wastewater into subsurface formations (Horton, 2012; Keranen and others, 2013; Hornbach and others, 2015); the largest earthquake likely induced by wastewater injection was the 2016 moment magnitude (M_w) 5.8 Pawnee, Okla., earthquake (Yeck and others, 2017). Hydraulic fracture stimulation of unconventional reservoirs, or fracking, has also induced felt earthquakes (Holland, 2013; Skoumal and oth-

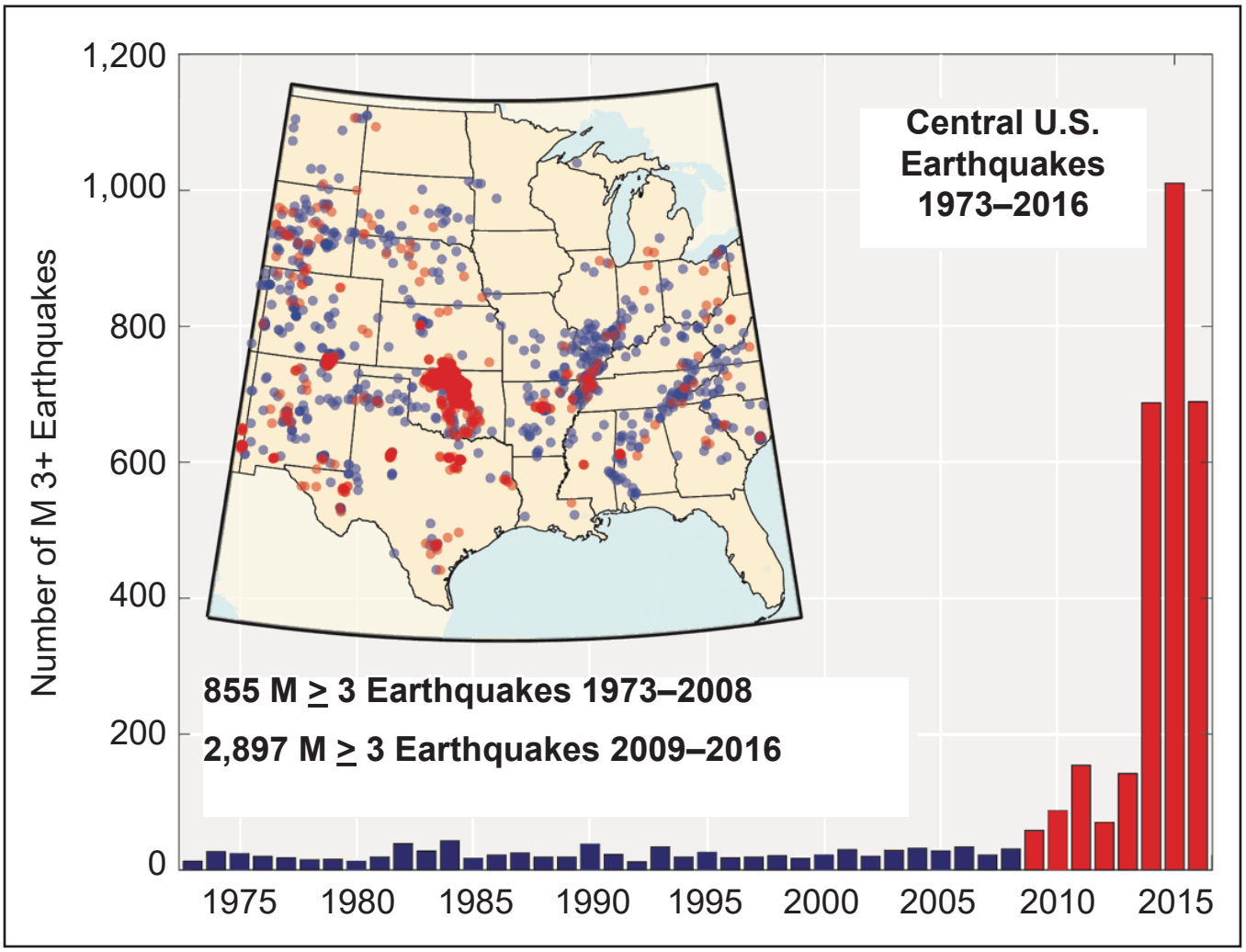

Figure 1. Annual number of magnitude 3 and greater earthquakes in the central United States (from earthquake.usgs.gov/research/induced/overview.php; last accessed 12/08/2017). The annual event count for years corresponding to the shale-gas boom beginning in 2009 are in red. Inset map shows earthquake epicenters during the same period; colors correspond to those in the bar graph.

ers, 2015; Bao and Eaton, 2016); the largest event likely induced by fracking was the 2015 M_w 3.9 Fox Creek earthquake in Alberta, Canada. Most cases of induced, felt earthquakes were the result of fluid injection into formations that are in hydraulic communication with the crystalline basement, which can lead to the rupture of preexisting, critically stressed basement faults (Zoback and others, 2002). The National Research Council (2013) presented an in-depth introduction to the issue of induced seismicity and the mechanisms involved.

In the Rome Trough of eastern Kentucky, the Rogersville Shale, a deep formation with total organic carbon content sufficient for hydrocarbon generation, has recently been tested in exploration wells (Harris, 2015). Because of its low permeability, the Rogersville Shale must be produced using unconventional methodologies—in particular, high-volume and high-pressure fracking. And, because this deep formation is in close proximity to the faulted, crystalline basement in the Rome Trough, there is a potential for fracking-induced earthquakes when oil and gas are produced from this shale.

In addition, produced wastewater has been injected in the eastern Kentucky Rome Tough since 1998 (Sparks and Curl, 2014). The injection formations in the Rome Trough are relatively shallow compared to the depth of the crystalline basement, and no injection-related events have been recorded by the regional seismic monitoring networks (Kentucky Geological Survey, 2014). If large-scale development of the Rogersville Shale occurs, and large volumes of brine are produced and injected, however, the risk of inducing earthquakes from wastewater disposal could increase.

Because the possibility of inducing earthquakes in the Rome Trough may increase if the Rogersville Shale becomes a productive hydrocarbon play, acquiring background microseismicity data in the area is important. In regions of concurrent subsurface fluid injection and seismic activity, unequivocally discriminating between natural and induced earthquakes requires the analysis of multiple data sets, including at minimum fluid-injection volume histories of active wastewater-disposal wells and an earthquake catalog. When the timing of earthquakes that occur near wastewater-injection wells and fracture stimulations is strongly correlated with the injection history, the probability of a causal relationship between the two increases. Also, cataloged seismicity-rate changes permit determining the probability that an increase in seismic activity is natural (Rubinstein and others, 2014). Natural and induced microearthquakes (earthquakes of magnitude less than 2.5) occur exponentially more frequently than larger, felt earthquakes, and are therefore a more sensitive indicator of variations in seismicity rate. Therefore, the background rates of microearthquakes are of particular importance for calculating the likelihood that earthquake activity is induced. Permanent, regional seismic monitoring stations are sparse, however, and if induced earthquakes were to occur in the Rome Trough from subsurface fluid injection, the existing regional stations would not permit the determination of event hypocenters (latitude, longitude, and focal depth) with sufficient accuracy and precision to suggest association of earthquakes with subsurface injection activities.

Consequently, the Eastern Kentucky Microseismic Monitoring Project was conceived soon after the first deep Rogersville Shale test well was completed in May 2014 in Lawrence County. The project features a network of sensitive seismic monitoring stations that were deployed in the Rome Trough to monitor the area around clusters of existing wastewater-injection wells and the most likely areas of oil and gas production from the Rogersville Shale. A seismicity catalog has been developed from the first two years of operation of the entire network (June 2016 through June 2018), and natural, background seismicity has been characterized with unprecedented detail. As of the time of publication of this report, the network remains in operation.

Project Setting

This project focuses on the Rome Trough of eastern Kentucky in the vicinity of active wastewater-injection wells and the area in which the Rogersville Shale is most likely to be tested and potentially developed. Because of the increased event-detection sensitivity that the microseismic monitoring network provides, the project area and its seismicity includes regions outside of the Rome Trough, approximately 50 km beyond the network

stations, and is bounded by latitude 37.1°N to 38.7°N and longitude 84.5°W to 82.0°W.

Geologic Setting

Tectonics and Regional Stress. The study area (Fig. 2) is in a stable continental region of the central Appalachian foreland basin of North America. It is underlain by a series of continental grabens that are collectively part of a more extensive interior failed rift system associated with the breakup of the supercontinent Rodinia during the Early and Middle Cambrian (Gao and others, 2000; Hickman, 2011). The Rome Trough, a northeast-trending graben system, is part of this larger failed Cambrian rift system extending from eastern Kentucky northeastward across West Virginia and Pennsylvania into southern New York (Harris and others, 2004; Hickman, 2011). As a result of the crustal extension of the interior rift system, a thick sequence of Cambrian sedimentary rocks is present in several grabens below the Appalachian foreland basin in eastern North America (Hickman, 2011).

In eastern Kentucky, the Rome Trough is bounded on the west by the Lexington Fault System, on the north by the Kentucky River Fault System, and on the south by the Rockcastle River Fault System (White, 2001). Although the Rome Trough does not coincide with a known zone of seismicity, it is adjacent to more seismically active zones to the

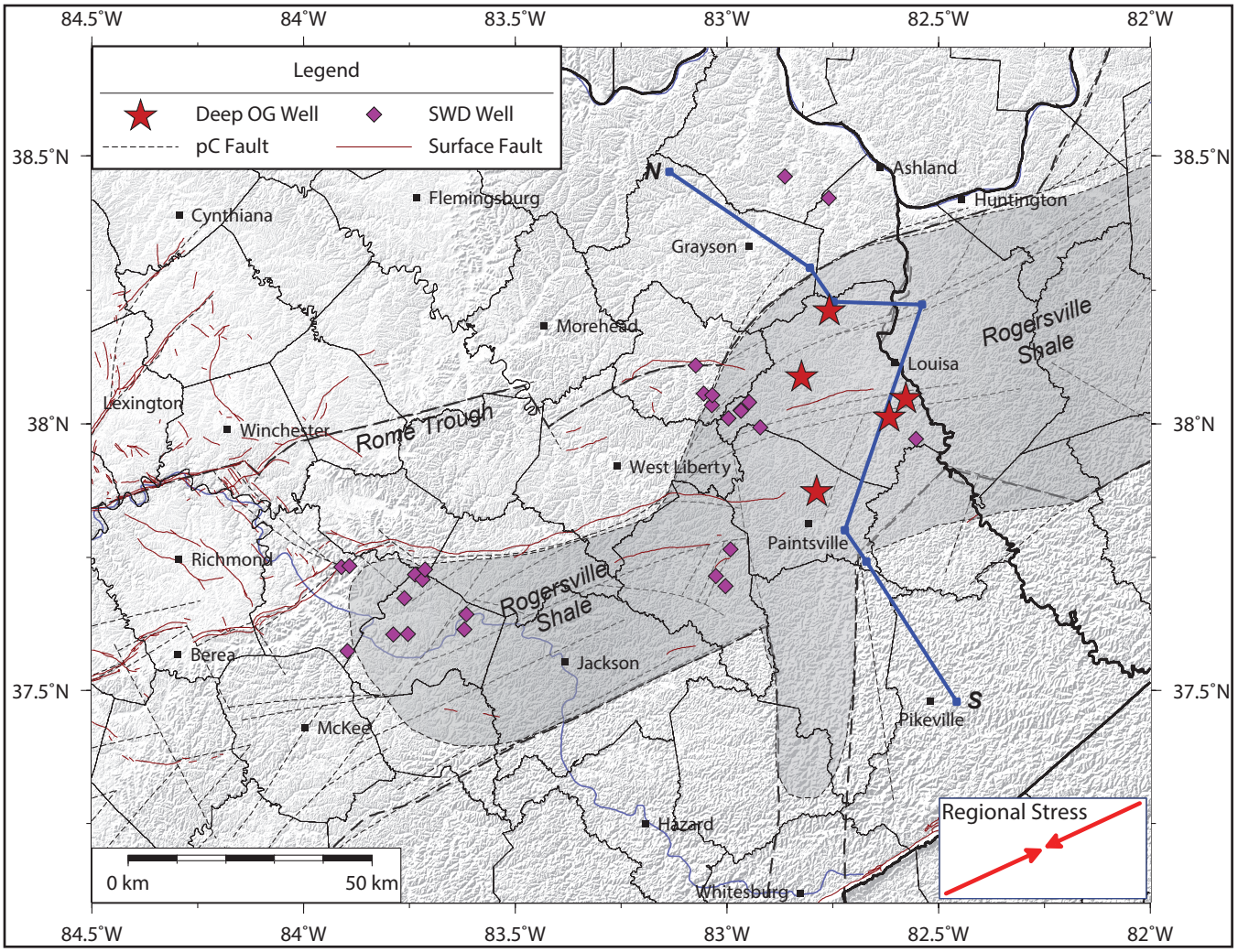

Figure 2. Surface and Precambrian (pC) faults, the Rome Trough boundary (heavy, dashed black lines), area of possible Rogersville Shale production (gray, shaded), and deep Rogersville Shale test wells (Deep OG Well) and wastewater-disposal wells (SWD well). Blue line is the location of the cross section shown in Figure 3. Red arrows in the inset show the direction of maximum horizontal regional stress.

north and to the south. The current maximum horizontal regional stress is compressive and oriented predominantly southwest-northeast, at roughly N60°E (Zoback and Zoback, 1989; Heidbach and others, 2008).

Major horizontal extension within the Rome Trough occurred from the end of the Precambrian through the Middle Cambrian, and is associated with the active rifting during the breakup of the supercontinent Rodinia. Volcanism within the Blue Ridge Rift between Laurentia and Amazonia evolved into the Mid-Iapetan Ridge to the southeast of the Rome Trough, and the southeastern rifted edge of Laurentia had developed into a passive margin by the Early Cambrian (Sloss, 1988).

Stratigraphy. In the Early to Middle Cambrian, sea level rose and flooded the graben, leading to the deposition of thick, arkosic synrift siliciclastic successions known as the Rome Formation. By the Middle Cambrian, the sea level had risen and the entire region was covered in a shallow sea. The Conasauga Group, consisting of deeper-water, low-energy siltstones and shales alternating with episodic carbonate deposits indicative of a slowly subsiding basin margin, was deposited during the Middle to Late Cambrian (Hickman, 2011). The Rogersville Shale is one of six formations recognized within the Conasauga Group and the only one that shows evidence of greater than 1 percent total organic carbon content (Hickman and others, 2015), generally regarded as the minimum required for commercial-grade hydrocarbon source rocks. The tectonic subsidence of the Rome Trough ended during the Late Cambrian, by which time sedimentation had filled the graben to the point that no topographic relief remained across the structure (Harris and others, 2004; Hickman, 2011).

From the Late Cambrian to the Early Ordovician, a regional carbonate platform known as the Great American Bank developed, replacing the clastic/episodic carbonate deposition seen in the Conasauga Group. This thick carbonate interval, the Knox Group, composed predominantly of carbonate (dolomitic) rocks with minor amounts of limestone and mature, quartz-rich sandstone, overlies the synrift strata of the entire graben system, as well as most of the Midcontinent region. In the Rome Trough, this group is between 1,500 and 3,400 ft thick. A short and intense regression followed this deposition, leading to subaerial exposure and erosion of Lower Ordovician dolomites and limestones, which produced the widespread post-Knox Unconformity (Sloss, 1988; Hickman, 2011).

In the Rome Trough study area, 1,300 to 14,000 ft of Middle Ordovician through Upper Pennsylvanian sediments overlie the Knox Unconformity, and thicken southeastward into the Appalachian Basin (Fig. 3).

Wastewater-Injection Wells

Class II wastewater-injection wells have operated in the Rome Trough of eastern Kentucky since at least 1998 (Fig. 4). Table 1 shows the monthly (annual divided by 12), annual, and total cumulative wastewater-injection volumes and the maximum observed wellhead pressures for the wells operating within the project area, based on records acquired from the U.S. Environmental Protection Agency; the cumulative volumes are plotted in Figure 5. There are several inconsistencies in the EPA records (Sparks, 2016). The volumes and pressures shown in Table 1 are the corrected values: apparent duplicate entries were deleted, two different sets of data for the same well were added together and the injection volume over the entire year was averaged, the highest wellhead pressure in the original data was used as the maximum wellhead pressure, and all injection volumes were converted to units of barrels.

Recent Unconventional Oil and Gas Exploration of the Rogersville Shale

In 2002, the U.S. Geological Survey and the Kentucky Geological Survey collaborated in a research project (the Rome Trough Consortium) and found that whole core from the Exxon No. 1 Smith well in Wayne County, W.Va., contained up to 4 weight-percent of organic carbon, indicating that the Rogersville Shale of the Cambrian Conasauga Group was a potential source rock for hydrocarbons. Unfortunately, at that time production from unconventional oil and gas exploration was limited, and so the resource potential from shale production was not considered in that study. In the following 11 years, however, the United States witnessed the "Shale Revolution," resulting in the

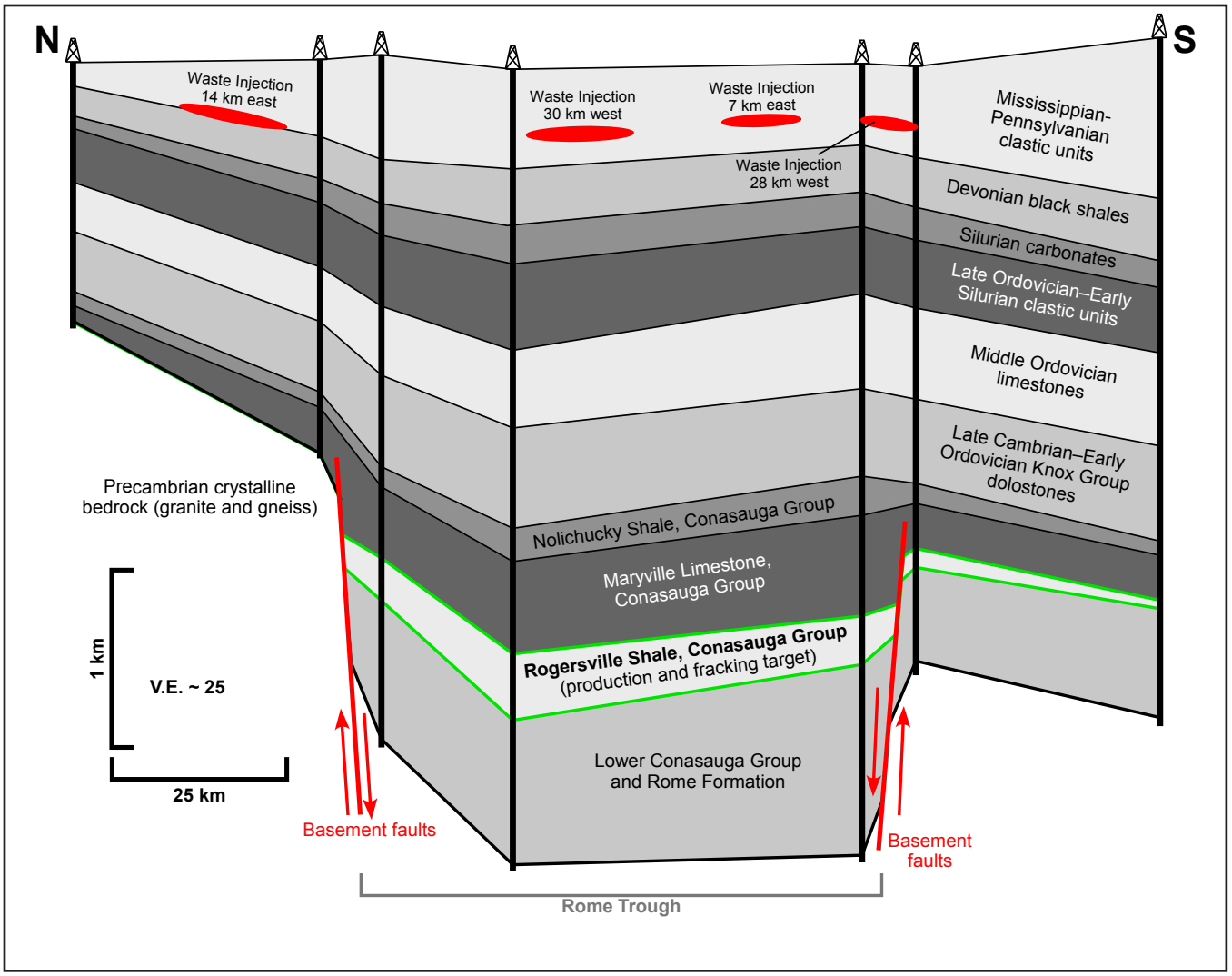

Figure 3. Cross section based on drillers' logs, with generalized stratigraphic groups, across the Rome Trough through the study area in eastern Kentucky and southwestern West Virginia (Fig. 2). Areas marked in red refer to depths of waste-injection targets within 30 km of the section. The Rogersville Shale, the target horizon for deep fracking, is outlined in green.

proliferation of advanced horizontal drilling and multistage hydraulic-fracturing techniques.

In the fall of 2013, Bruin Exploration (a wholly owned subsidiary of the Cimarex Corp. in Denver) permitted and drilled the No. 1 Sylvia Young well in Lawrence County, Ky., specifically to test the exploration potential of the Rogersville Shale. Since the completion of the Young well, five more wells targeting the Rogersville have been drilled in the Rome Trough of Kentucky and West Virginia (Fig. 2): the Bruin Exploration No. 1H Walbridge horizontal well, Chesapeake Appalachia's No. LAW-1 Stephens and No. LAW-1 Northup (the deepest in Kentucky) wells, the Horizontal Technology No. 572361 EQT Production well, and the Cabot Oil & Gas No. 50 Amherst Industries well in Putnam County, W.Va., which is currently shut-in after producing 340 million cubic feet of gas from the Rogersville through December 2017.

Regional Seismic Monitoring and Historical Seismicity

Prior to 1980, seismic monitoring in the vicinity of the project area was sparse and intermittent, which resulted in variable minimum magnitudes (M_{min}) of detectable earthquakes in the region. Soon after the 1980 M_w 5.0 Sharpsburg earthquake, the first long-term, continuous seismic monitoring stations within 100 km of the Rome Trough of eastern Kentucky were installed by the University of

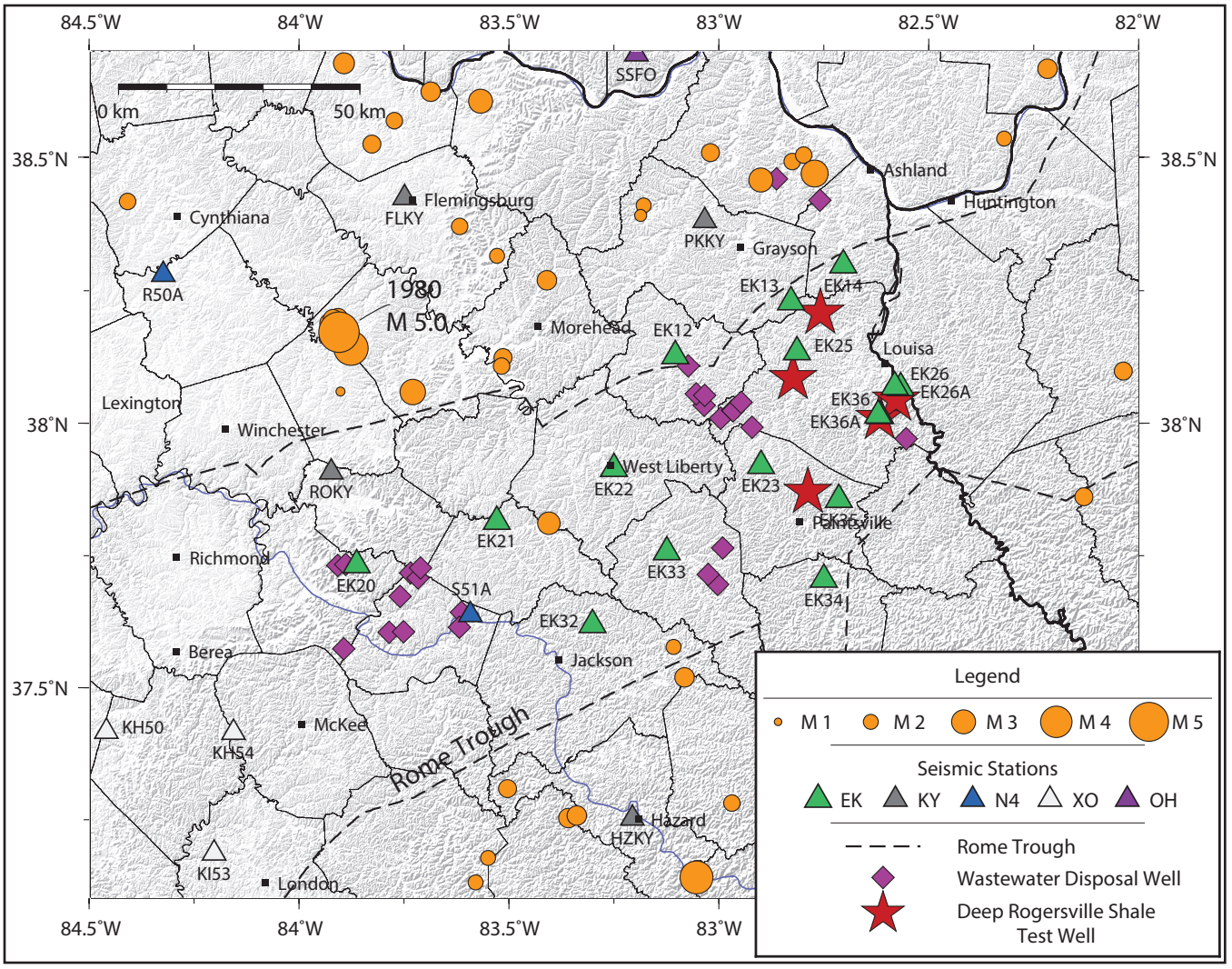

Figure 4. Seismicity since 1980, operational UIC Class II wastewater-injection wells, Rogersville Shale oil and gas test wells, Eastern Kentucky Microseismic Monitoring network stations (EK), seismic stations operating during at least part of the microseismic network operation (see Tables 2 and 3 for network codes), and the boundary of the Rome Trough.

Kentucky (Table 2), and by 1985, UK was operating three stations in the region. The M_{min} maps in Figure 6 show estimated detection thresholds in the project area (calculated according to the procedure discussed in the Detection Threshold Modeling section) prior to deployment of the microseismic network. The estimated detection threshold ranged from M_w 1.5 in the southwestern Rome Trough to M_w 1.9 in the northeastern Rome Trough for long-term, regional seismic stations (not all stations are shown on the maps). With the addition of temporary EarthScope (Central and Eastern United States Network) stations, which were operational at the time of the microseismic monitoring project, the detection thresholds ranged from M_w 1.5 to 1.7 in the same area.

The U.S. Geological Survey's Advanced National Seismic System Comprehensive Earthquake Catalog (earthquake.usgs.gov/earthquakes/search; last searched 12/08/2017) (Fig. 4) includes events located with stations listed in Table 2 as well as stations that are either no longer operating or are more distant, long-term, regional stations. Occasionally, the recordings from other nearby stations temporarily deployed for special projects were used to locate events in the catalog. Thus, the ANSS Comprehensive Catalog is not a uniform catalog of events (in other words, a catalog of events observed with uniform monitoring sensitivity) in

Table 1. Kentucky Class II injection well data (September 1997–December 2016).

EPA ID	*Latitude (decimal degrees)*	*Longitude (decimal degrees)*	*Depth (ft)*	*Injection Interval or Formation*	*Start Date (mm/yyyy)*	*End Date (mm/yyyy)*	*Maximum Pressure (psig)*	*Annual Injection Volume (bbl)*	*Average Monthly Injection Volume (bbl)*	*Cumulative Injection Volume (bbl)*
KYS0430001	38.360008	82.829812	1,268	Berea Sandstone	12/2013	12/2013		1,818	1,818	171,303
					01/2014	12/2014	820	103,384	8,615.3	
					01/2016	12/2016	867	66,101	5,508.4	
KYS0630001	38.034951	83.03576	1,103	Weir Sandstone	01/1999	12/1999	440	715	59.6	51,286
					01/2000	12/2000	490	581	48.4	
					01/2001	12/2001	345	0	0.0	
					01/2002	12/2002	0	0	0.0	
					01/2003	12/2003	0	0	0.0	
					01/2005	12/2005	500	5,380	448.3	
					01/2006	12/2006	500	15,695	1,307.9	
					01/2007	12/2007	590	5,235	436.3	
					01/2008	12/2008	570	4,945	412.1	
					01/2010	12/2010	580	1,715	142.9	
					01/2011	12/2011	575	6,270	522.5	
					01/2012	12/2012	560	4,415	367.9	
					01/2013	12/2013	0	4,545	378.8	
					01/2014	12/2014	550	1,790	149.2	

Table 1. Kentucky Class II injection well data (September 1997–December 2016).

EPA ID	*Latitude (decimal degrees)*	*Longitude (decimal degrees)*	*Depth (ft)*	*Injection Interval or Formation*	*Start Date (mm/yyyy)*	*End Date (mm/yyyy)*	*Maximum Pressure (psig)*	*Annual Injection Volume (bbl)*	*Average Monthly Injection Volume (bbl)*	*Cumulative Injection Volume (bbl)*
KYS0630003	38.057136	83.054624	838	Weir Sandstone	01/1999	12/1999		10	0.8	24,266
					01/2000	12/2000	0	2,328	194.0	
					01/2001	12/2001	0	4,113	342.8	
					01/2002	12/2002	0	4,682	390.2	
					01/2003	12/2003	380	4,273	356.1	
					01/2004	12/2004	250	3,417	284.8	
					01/2005	12/2005	300	4,465	372.1	
					01/2006	12/2006	300	978	81.5	
					01/2007	12/2007	0	0	0	
					01/2008	12/2008	0	0	0	
					01/2009	12/2009	0	0	0	
					01/2010	12/2010	0	0	0	
KYS0630004	38.05376	83.034645	958	Weir Sandstone	11/1999	12/2000	765	17,763	1,268.8	203,990
					01/2001	12/2001	750	15,907	1,325.6	
					01/2002	12/2002	780	14,320	1,193.3	
					01/2003	12/2003	750	15,675	1,306.3	
					01/2004	12/2004	745	19,131	1,594.3	
					01/2005	12/2005	745	15,061	1,255.1	
					01/2006	12/2006	750	15,554	1,296.2	
					01/2007	12/2007	730	20,414	1,701.2	
					01/2008	12/2008	730	14,407	1,200.6	
					01/2009	12/2009	735	16,011	1,334.3	
					01/2010	12/2010	736	13,731	1,144.3	
					01/2011	12/2011	735	13,951	1,163.1	
					01/2012	12/2012	735	0	0.0	
					01/2013	12/2013	735	0	0.00	
					01/2014	12/2014	735	12,059	1,004.9	

Table 1. Kentucky Class II injection well data (September 1997–December 2016).

EPA ID	*Latitude (decimal degrees)*	*Longitude (decimal degrees)*	*Depth (ft)*	*Injection Interval or Formation*	*Start Date (mm/yyyy)*	*End Date (mm/yyyy)*	*Maximum Pressure (psig)*	*Annual Injection Volume (bbl)*	*Average Monthly Injection Volume (bbl)*	*Cumulative Injection Volume (bbl)*
KYS0630007	38.109284	83.07422	3,230	Weir Sandstone	01/1999	12/1999	350	11,439	953.3	206,367
					01/2000	12/2000	250	9,665	805.4	
					01/2001	12/2001	250	8,177	681.4	
					01/2002	12/2002	250	7,470	622.5	
					01/2003	12/2003	225	7,270	605.8	
					01/2004	12/2004	200	12,420	1,035.0	
					01/2005	12/2005	225	5,393	449.4	
					01/2006	12/2006	125	7,349	612.4	
					01/2007	12/2007	200	6,456	538.0	
					01/2008	12/2008	225	19,196	1,599.7	
					01/2009	12/2009	440	52,780	4,398.3	
					09/2011	12/2011	320			
					01/2012	12/2012	320	22,080	1,840.0	
					01/2013	12/2013	0	16,123	1,343.6	
					01/2014	12/2014		20,549	1,712.4	
KYS0650091	37.717902	83.736737	786	Corniferous	09/1997	08/1998		0	0.0	1,850
					09/1998	12/2011		no reported activity		
					01/2012	12/2012	0	1,850	154.2	
					01/2013	12/2013	0	0		
					01/2014	12/2014	0	0		

Table 1. Kentucky Class II injection well data (September 1997–December 2016).

EPA ID	*Latitude (decimal degrees)*	*Longitude (decimal degrees)*	*Depth (ft)*	*Injection Interval or Formation*	*Start Date (mm/yyyy)*	*End Date (mm/yyyy)*	*Maximum Pressure (psig)*	*Annual Injection Volume (bbl)*	*Average Monthly Injection Volume (bbl)*	*Cumulative Injection Volume (bbl)*
KYS0650118	37.732667	83.910361	2,580	Knox Group	01/2009	12/2009	750	3,818	318.2	569,031
					01/2010	12/2010	750	103,783	8,648.6	
					01/2011	12/2011	750	64.658	5,388.2	
					01/2012	12/2012		112,151	9,345.9	
					01/2013	12/2013	750	110,914	9,242.8	
					01/2014	12/2014	750	104,616	8,718.0	
					01/2015	12/2015	750	69,091	5,757.6	
KYS0650119	37.73435	83.89221	2,632	Knox Group	01/2008	12/2008	0	0		121,525
					01/2009	12/2009	750	3,560	296.7	
					01/2010	12/2010		38,434	3,202.8	
					01/2011	12/2011	300	27,729	2,310.8	
					01/2012	12/2012	300	12,503	1,041.9	
					01/2013	12/2013	300	22,303	1,858.6	
					01/2014	12/2014	300	16,996	1,416.3	
KYS0650123	37.573914	83.896129	3,163	Knox Group	01/2016	12/2016	0	135	11.3	135
KYS0890002	38.4618	82.862621	900	Berea Sandstone	01/2001	12/2001	500	240	20	184,444
					01/2002	12/2002	550	12,811	1,067.6	
					01/2003	12/2003	550	10,770	897.5	
					01/2004	12/2004	550	9,540	795.0	
					01/2005	12/2005	520	9,690	807.5	
					01/2007	12/2007	200			
					01/2012	12/2012	900	10,796	899.7	
					01/2013	12/2013	790	39,745	3,312.1	
					01/2014	12/2014	810	48,309	4,025.8	
					01/2016	12/2016	835	42,543	3,545.3	

Table 1. Kentucky Class II injection well data (September 1997–December 2016).

EPA ID	*Latitude (decimal degrees)*	*Longitude (decimal degrees)*	*Depth (ft)*	*Injection Interval or Formation*	*Start Date (mm/yyyy)*	*End Date (mm/yyyy)*	*Maximum Pressure (psig)*	*Annual Injection Volume (bbl)*	*Average Monthly Injection Volume (bbl)*	*Cumulative Injection Volume (bbl)*
KYS1270039	38.010773	82.996659	995	Weir Sandstone	01/1999	12/1999				69,875
					01/2000	12/2000	475	1,200	100.0	
					01/2001	12/2001	425	15	1.3	
					01/2002	12/2005	0	no reported activity		
					01/2006	12/2006	425	150	12.5	
					01/2009	12/2009	300	16,957	1,413.1	
					01/2010	12/2010	500	20,795	1,732.9	
					01/2011	12/2011	618	10,609	884.1	
					01/2012	12/2012	550	1,210	100.8	
					01/2013	12/2013	500	11,819	984.9	
					01/2014	12/2014	600	6,000	500.0	
					01/2015	12/2015	550	1,120	93.3	
KYS1270162	38.025895	82.967748	1,024	Weir Sandstone	01/2000	12/2000	405	17,166	1,430.5	166,546
					01/2001	12/2001	455	16,794	1,399.5	
					01/2002	12/2002	470	16,201	1,350.1	
					01/2003	12/2003	400	16,470	1,372.5	
					01/2004	12/2004	340	24,183	2,015.3	
					01/2005	12/2005	430	24,392	2,032.7	
					01/2006	12/2006	405	13,128	1,094.0	
					01/2007	12/2007	510	9,516	793.0	
					01/2008	12/2008	375	13,064	1,088.7	
					01/2010	12/2010	470	5,160	430.0	
					01/2011	12/2011	430	4,967	413.9	
					01/2012	12/2012	360	1,818	151.5	
					01/2015	12/2015	425	3,687	307.3	

Table 1. Kentucky Class II injection well data (September 1997–December 2016).

EPA ID	*Latitude (decimal degrees)*	*Longitude (decimal degrees)*	*Depth (ft)*	*Injection Interval or Formation*	*Start Date (mm/yyyy)*	*End Date (mm/yyyy)*	*Maximum Pressure (psig)*	*Annual Injection Volume (bbl)*	*Average Monthly Injection Volume (bbl)*	*Cumulative Injection Volume (bbl)*
KYS1270163	38.024818	82.966453	1,231	Weir Sandstone	01/2000	12/2000	305	14,045	1,170.4	96,909
					01/2001	12/2001	355	13,730	1,144.2	
					01/2002	12/2002	360	13,263	1,105.3	
					01/2003	12/2003	235	13,486	1,123.8	
					01/2004	12/2004	300	5,921	493.4	
					01/2005	12/2005	265	2,272	189.3	
					01/2006	12/2006	325	8,740	728.3	
					01/2007	12/2007	185	6,348	529.0	
					01/2008	12/2008	200	8,516	709.7	
					01/2010	12/2010	320	3,602	300.2	
					01/2011	12/2011	330	3,317	276.4	
					01/2012	12/2012	225	1,210	100.8	
					01/2015	12/2015	320	2,459	204.9	
KYS1270202	37.97237	82.55358	1,086	Lee Sandstone	01/1999	12/1999	500	9,266	772.2	32,370
					01/2001	12/2001	500	5,332	444.3	
					01/2002	12/2002	500	4,173	347.8	
					01/2003	12/2003	500	5,599	466.6	
					01/2006	12/2006	500	740	61.7	
					01/2007	12/2007	500	7,260	605.0	

Table 1. Kentucky Class II injection well data (September 1997–December 2016).

EPA ID	*Latitude (decimal degrees)*	*Longitude (decimal degrees)*	*Depth (ft)*	*Injection Interval or Formation*	*Start Date (mm/yyyy)*	*End Date (mm/yyyy)*	*Maximum Pressure (psig)*	*Annual Injection Volume (bbl)*	*Average Monthly Injection Volume (bbl)*	*Cumulative Injection Volume (bbl)*
KYS1270203	38.040946	82.948106	1,070	Weir Sandstone	01/2000	12/2000	210	1,487	123.9	94,856
					01/2001	12/2001	210	13,637	1,136.4	
					01/2002	12/2002	210	13,100	1,091.7	
					01/2003	12/2003	185	13,401	1,116.8	
					01/2005	12/2005	190	14,871	1,239.3	
					01/2006	12/2012	0	no reported activity		
					01/2013	12/2013	175	5,875	489.6	
					01/2014	12/2014	220	18,104	1,508.7	
					01/2016	12/2016	145	14,381	1,198.4	
KYS1270329	37.99385	82.92188	990	Weir Sandstone	01/2010	12/2010	650	55	4.6	27,167
					01/2011	12/2011	660	5,782	481.8	
					01/2012	12/2012	660	9,597	799.8	
					01/2013	12/2013	660	4,707	392.3	
					01/2014	12/2014	650	2,827	235.6	
					01/2015	12/2015	650	4,199	349.9	
KYS1290092	37.603807	83.754965	1,224	Lockport Dolomite	08/1998	07/1998		5,120	426.7	19,180
					08/1999	12/1999		1,780	356.0	
					01/2000	12/2000		4,770	397.5	
					01/2001	12/2001		4,300	358.3	
					01/2002	12/2002		3,210	267.5	

Table 1. Kentucky Class II injection well data (September 1997–December 2016).

EPA ID	*Latitude (decimal degrees)*	*Longitude (decimal degrees)*	*Depth (ft)*	*Injection Interval or Formation*	*Start Date (mm/yyyy)*	*End Date (mm/yyyy)*	*Maximum Pressure (psig)*	*Annual Injection Volume (bbl)*	*Average Monthly Injection Volume (bbl)*	*Cumulative Injection Volume (bbl)*
KYS1290843	37.60542	83.78781	1,202	Corniferous	01/2000	12/2000		549	45.8	31,367
					01/2001	12/2001	0			
					01/2002	12/2002		75	6.3	
					01/2010	12/2010	0	8,960	746.7	
					01/2011	12/2011	0	10,830	902.5	
					01/2012	12/2012	0	5,840	486.7	
					01/2014	12/2014	0	4,800	400.0	
					01/2016	12/2016	0	313	26.1	
KYS1290892	37.643009	83.615108	1,130	Lockport Dolomite	01/2000	12/2006	0	no reported activity		97,385
					01/2007	12/2007	800	37,802	3,150.2	
					01/2008	12/2008	800	23,736	1,978.0	
					01/2009	12/2009	780	18,304	1,525.3	
					01/2011	12/2011	700	10,569	880.8	
					01/2012	12/2012	800	6,974	581.2	
					01/2013	12/2013	0			
					01/2014	12/2014	0			

Table 1. Kentucky Class II injection well data (September 1997–December 2016).

EPA ID	*Latitude (decimal degrees)*	*Longitude (decimal degrees)*	*Depth (ft)*	*Injection Interval or Formation*	*Start Date (mm/yyyy)*	*End Date (mm/yyyy)*	*Maximum Pressure (psig)*	*Annual Injection Volume (bbl)*	*Average Monthly Injection Volume (bbl)*	*Cumulative Injection Volume (bbl)*
KYS1291166	37.708293	83.719331	873	Lockport Dolomite	09/1998	12/1998	0	33,208	8,302.0	317,829
					01/1999	12/1999	0	70,589	5,882.4	
					01/2000	12/2000	0	11,815	984.6	
					01/2001	08/2001	0	6 ,937	867.1	
					01/2002	12/2002	0	9,738	811.5	
					01/2003	12/2003	0	20,500	1,708.3	
					01/2004	12/2004	0	16,991	1,415.9	
					01/2005	12/2005		37,108	3,092.3	
					01/2006	12/2006	0			
					01/2007	12/2007	0	13,738	1,144.8	
					01/2008	12/2008	0	29,827	2,485.6	
					01/2009	12/2009	0	55,075	4,589.6	
					01/2010	12/2010	0			
					01/2011	12/2011	0			
					01/2012	12/2012	0	1,850	154.2	
					01/2014	12/2014	0	10,453	871.1	
KYS1292147	37.606349	83.753817	1,200	Lockport Dolomite	01/2003	12/2003	0	3,800	316.7	41,040
					01/2004	12/2004	0	3,700	308.3	
					01/2005	12/2005	0	3,675	306.3	
					01/2006	12/2006		3,600	300.0	
					01/2007	12/2007	0	3,600	300.0	
					01/2008	12/2008	0	3,600	300.0	
					01/2009	12/2009	0	3,600	300.0	
					01/2010	12/2010	0	3,880	323.3	
					01/2011	12/2011		3,810	317.5	
					01/2012	12/2012	0	3,900	325.0	
					01/2014	12/2014	0	3,875	322.9	

Table 1. Kentucky Class II injection well data (September 1997–December 2016).

EPA ID	*Latitude (decimal degrees)*	*Longitude (decimal degrees)*	*Depth (ft)*	*Injection Interval or Formation*	*Start Date (mm/yyyy)*	*End Date (mm/yyyy)*	*Maximum Pressure (psig)*	*Annual Injection Volume (bbl)*	*Average Monthly Injection Volume (bbl)*	*Cumulative Injection Volume (bbl)*
KYS1292152	37.615361	83.619833	4,570	Rose Run Sandstone, upper part of Knox Group	01/2009	12/2009		373,535	31,127.9	1,730,917
					01/2011	12/2011	0	407,153	33,929.4	
					01/2012	12/2012	0	416,250	34,687.5	
					01/2013	12/2013	0	298,937	24,911.4	
					01/2014	12/2014	0	235,042	19,586.8	
KYS1292154	37.64899	83.63379	3,975	Beekmantown Dolomite, upper part of Knox Group	01/2012	12/2012	135	108,171	9,014.3	604,379
					01/2013	12/2013		232,621	19,385.1	
					01/2014	12/2015		263,587	21,965.6	
KYS1292155	37.673554	83.761668	3,297	Beekmantown Dolomite, upper part of Knox Group	01/2012	12/2012	600	2,400	342.9	20,550
					01/2013	12/2013	600	8,350	695.8	
					01/2014	12/2014	600	9,800	816.7	
KYS1530298	37.696177	83.003804	1,204	Weir Sandstone	10/2014	12/2014	755	1,305	435.0	57,292
					01/2014	12/2014	735	28,841	2,403.4	
					01/2015	12/2015	800	27,146	2,262.2	
KYS1530299	37.715815	83.026594	1,400	Weir Sandstone	01/2014	12/2014	800	18,115	1,509.6	18,115
KYS1970344	37.728019	83.712847	894	Lockport Dolomite	09/1998	12/1998	0	379	94.8	5,374
					01/1999	08/1999	0	758	94.8	
					01/2000	12/2011	0	no reported activity		
					01/2012	12/2012	0	265	22.1	
					01/2014	12/2014	0	3,972	331.0	

Table 1. Kentucky Class II injection well data (September 1997–December 2016).

EPA ID	*Latitude (decimal degrees)*	*Longitude (decimal degrees)*	*Depth (ft)*	*Injection Interval or Formation*	*Start Date (mm/yyyy)*	*End Date (mm/yyyy)*	*Maximum Pressure (psig)*	*Annual Injection Volume (bbl)*	*Average Monthly Injection Volume (bbl)*	*Cumulative Injection Volume (bbl)*
KYS2370104	37.713537	83.69828	1,211	Lockport Dolomite	09/1998	12/1998		924	231.0	44,526
					01/1999	12/1999		3,214	267.8	
					01/2000	12/2000		5,753	479.4	
					01/2001	12/2001		6,041	755.1	
					01/2002	12/2002	0	8,303	691.9	
					01/2003	12/2003		2,306	192.2	
					01/2004	12/2004	0	1,811	150.9	
					01/2005	12/2005		1,565	130.4	
					01/2006	12/2006	0	2,259	188.3	
					01/2007	12/2007	0	1,614	134.5	
					01/2008	12/2008	0	2,325	193.8	
					01/2009	12/2009	0	5,192	432.7	
					01/2010	12/2010		815	67.9	
					01/2011	12/2011	0	254	21.2	
					01/2012	12/2012	0	1,850	154.2	
					01/2013	12/2013	0	300	25.0	
					01/2014	12/2014	0	0		

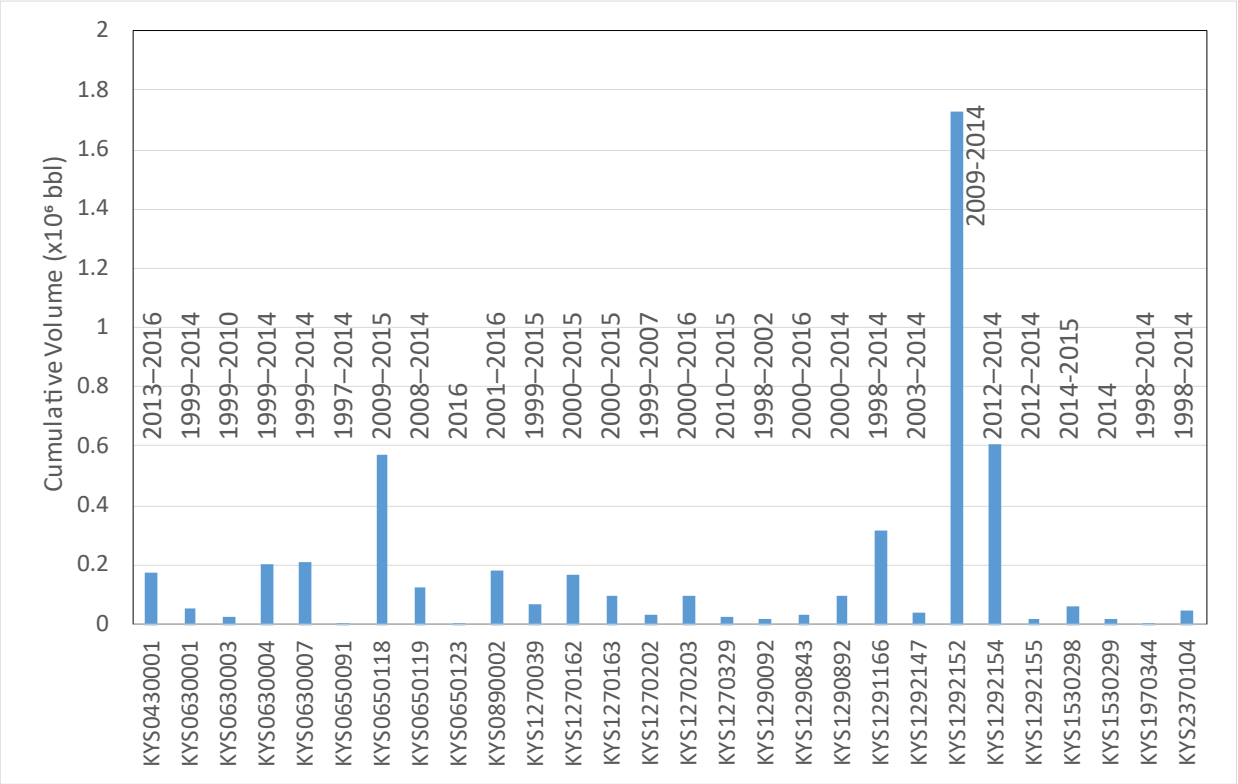

Figure 5. Cumulative injection volumes (in barrels) from UIC Class II wastewater-injection wells operating in the project area (Fig. 4). X-axis labels are EPA identification numbers. Plot labels are the range of years over which the cumulative volumes were calculated.

Table 2. Long-term, continuous seismic monitoring stations within 100 km of the Rome Trough of eastern Kentucky. Year On = year of installation or the year when data acquisition at KGS began, whichever is later. ET = Southern Appalachian Seismic Network, Center for Earthquake Research and Information, University of Memphis (www.fdsn.org/networks/detail/ET; last accessed 12/14/2018). KY = Kentucky Seismic and Strong-Motion Network (doi:10.7914/SN/KY; last accessed 12/14/2018). OH = Ohio Seismic Network (doi:10.7914/SN/OH; last accessed 12/14/2018). US = United States National Seismic Network (doi:10.7914/SN/US; last accessed 12/14/2018). CT = coincidence triggering. BINDER = grid-based phase-arrival detection associator (Earthworm's BINDER module). None = not for event triggering.

Station	*Network*	*County, State*	*Latitude*	*Longitude*	*Year On*	*Triggering Algorithm*
BHKY	KY	Fayette, Ky.	38.0344	–84.5032	1982	CT
FLKY	KY	Fleming, Ky.	38.4261	–83.7506	1989	CT, BINDER
HZKY	KY	Perry, Ky.	37.2511	–83.2067	2012	CT, BINDER
PKKY	KY	Carter, Ky.	38.3830	–83.0341	1985	CT, BINDER
ROKY	KY	Powell, Ky.	37.9091	–83.9257	1985	CT, BINDER
ASTN	ET	Grainger, Tenn.	36.3270	–83.4760	2009	none
LRVA	ET	Lee, Va.	36.7880	–82.7860	2012	none
WMTN	ET	Campbell, Tenn.	36.4100	–84.1760	2009	none
SSFO	OH	Scioto, Ohio	38.6953	–83.1972	2017	CT, BINDER
TZTN	US	Claiborne, Tenn.	36.5439	–83.5490	2010	CT

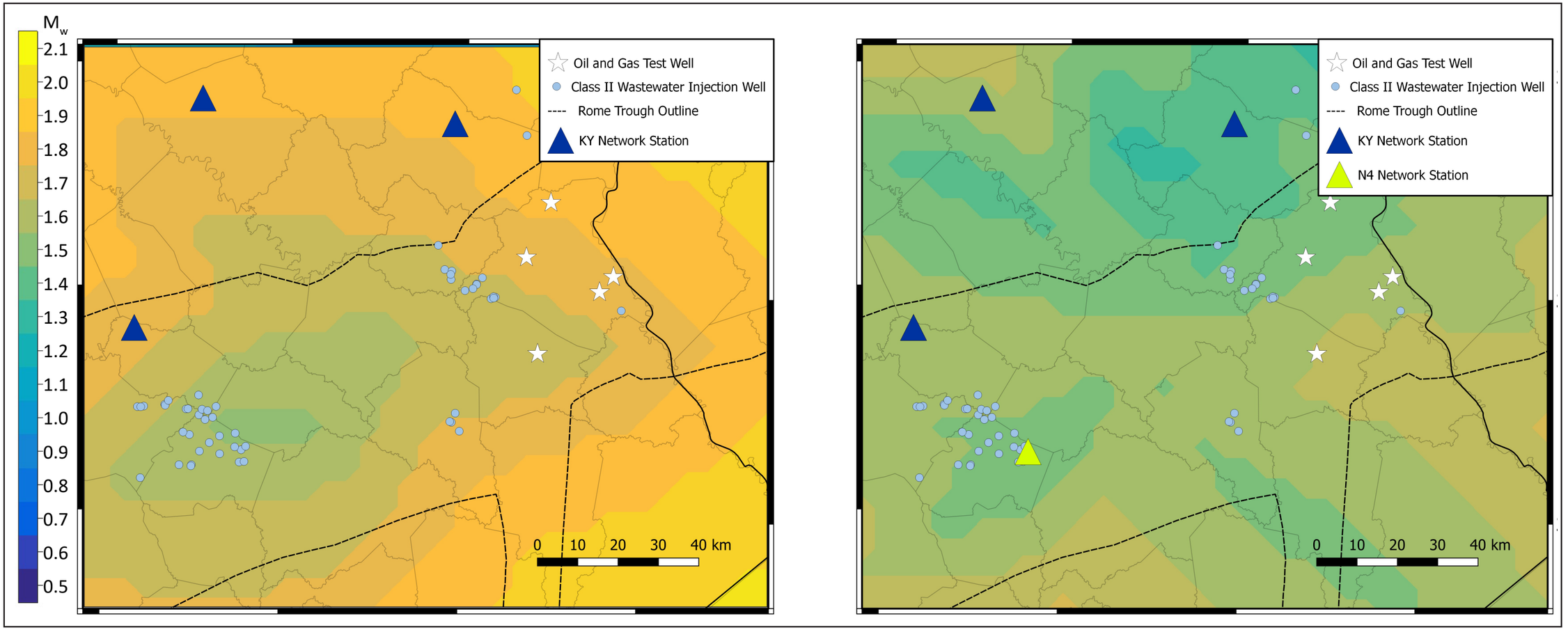

Figure 6. Minimum detectable earthquake magnitude in the project area prior to the deployment of the microseismic network: Detection threshold prior to the installation of the EarthScope USArray stations (left). Detection threshold including the EarthScope USArray stations (right). KY and N4 are the network codes for the Kentucky Seismic and Strong-Motion Network and Central and Eastern United States Network (www.usarray.org/ceusn; last accessed 12/14/2018), respectively.

the study area. However, it was used as the reference catalog in this report, for comparison with our microseismic monitoring earthquake catalog.

Since 1980, seismicity in the project area is characterized by a diffuse distribution of small-magnitude events outside of the Rome Trough of eastern Kentucky. Exceptions to this are the 1980 M_w 5.0 Sharpsburg, Ky., earthquake (Herrmann and others, 1982) to the north of the Rome Trough and the 2012 M_w 4.2 Perry County earthquake to the south, which is located in the northern part of the Eastern Tennessee Seismic Zone (Carpenter and others, 2014). Within the Rome Trough of eastern Kentucky, only two earthquakes since 1980 are reported in the ANSS Comprehensive Catalog.

In addition to the long-term, continuously operating stations listed in Table 2, other short-term stations operated during at least part of the operation of the microseismic monitoring project; they are included in Table 3. Real-time recordings from these stations were used simultaneously with telemetered recordings from the microseismic monitoring project to improve the detectability and location accuracy of events outside of the Rome Trough. One station, S51A, was within the Rome Tough, however, and was incorporated into the microseismic monitoring network configuration.

Microseismicity Investigation

Temporary Monitoring Network

The principal component of the project is the seismic monitoring network (Fig. 4). Instrumentation for most of the network was purchased by the Kentucky Geological Survey, with support from the University of Kentucky Department of Earth and Environmental Sciences. Cimarex Energy Co. contributed six complete stations to the monitoring network, and Nanometrics, the manufacturer of the instruments used, contributed support for one station. Instrumentation in the microseismic monitor-

Table 3. Temporary seismic stations used in real-time monitoring. XO = OIINK EarthScope Flexible Array experiment (Yang and others, 2014). N4 = Central and Eastern United States Network (www.usarray.org/ceusn; last accessed 12/14/2018). TA = EarthScope Transportable Array (www.usarray.org/researchers/obs/transportable; last accessed 12/14/2018). On Date = date of installation or the date when data acquisition at KGS began, whichever is later. Off Date = date of uninstallation; no date indicates that the station is still operational. CT = coincidence triggering. BINDER = grid-based phase-arrival detection associator (Earthworm's BINDER module).

Station	*Network*	*Latitude (°N)*	*Longitude (°E)*	*On Date*	*Off Date*	*Triggering Algorithm*
KH50	XO	37.4170	–84.4633	06/15/2015	10/17/2015	CT
KH54	XO	37.4149	–84.1600	06/15/2015	10/17/2015	CT
KI51	XO	37.1857	–84.5075	06/15/2015	10/17/2015	CT
KI53	XO	37.1845	–84.2061	06/15/2015	10/17/2015	CT
KJ50	XO	37.0462	–84.5808	06/15/2015	10/17/2015	CT
KJ52	XO	36.9186	–84.2500	06/15/2015	10/17/2015	CT
KK50	XO	36.8694	–84.8024	06/15/2015	10/17/2015	CT
P51A	N4	39.4818	–83.0601	06/15/2015		CT
P53A	N4	39.4868	–81.3896	06/15/2015		CT
Q51A	N4	39.0260	–83.3456	06/15/2015		CT, BINDER
Q52A	N4	38.9622	–82.2669	06/15/2015		CT, BINDER
R49A	N4	38.2916	–85.1714	04/12/2016		BINDER
R50A	N4	38.2816	–84.3274	06/15/2015		CT, BINDER
R53A	N4	38.3307	–81.9522	06/15/2015		CT, BINDER
S51A	N4	37.6392	–83.5935	06/15/2015		CT, BINDER
S54A	N4	37.7997	–81.3114	06/15/2015		CT, BINDER
T50A	N4	37.0204	–84.8384	06/15/2015		CT
U54A	N4	36.5209	–81.8204	06/15/2015		CT
P52A	TA	39.6337	–82.1325	06/15/2015		CT

ing network consists of broadband ground-motion sensors (corner periods of 40 s or lower and high-frequency cutoff of 85 Hz or higher) and 24-bit data loggers. Fourteen of the stations were equipped with cellular modems for data telemetry.

The real-time network layout was designed to provide monitoring coverage in the Rome Trough of eastern Kentucky in the vicinity of wastewater-injection wells and the deep exploration wells. Station distribution was slightly denser in the eastern part of the project area, where the Rogersville Shale is most likely to be tested and produced, because the wells that target the unconventional Rogersville Shale with high-volume hydraulic-fracture stimulations are closer to the crystalline basement than the wastewater-injection wells in the Rome Trough (Fig. 3), and may be more likely to induce earthquakes than the wastewater-disposal wells. Station installations began in June 2015, and the final real-time station was installed in February 2017 (Table 4). The station locations were determined to satisfy multiple criteria—including the identification of consenting landowners—that must be considered for the successful operation of telemetered, autonomous, broadband seismographs (Holcomb, 2017).

In addition to the 14 stations with real-time data telemetry, two additional stations without telemetry were deployed. These stations, EK26A and EK36A, were installed near Rogersville test wells prior to well completions: EK36A was installed three days prior to the multiple-stage frack of the Walbridge Holdings LLC well in Lawrence County and EK26A was installed south of Louisa prior to diagnostic fracture injection testing of the JH Northup Estate Inc. well. In both cases, the temporary station was operational during the hydraulic fracturing. Processing of the continuous recordings of these stations has not been completed as of the preparation of this report, and these stations did not contribute to the network triggering used for detecting the events presented in this report. Recordings from EK36A were used to analyze an earthquake in the Rome Trough, however. Various installation styles were used, depending on the instrumentation type installed (Table 4), the

Table 4. Eastern Kentucky Microseismic Monitoring network station locations, configurations, and operational time period.

Station	*Latitude (°N)*	*Longitude (°E)*	*Instrument*	*Installation Type*	*Data Telemetry*	*Date of Installation*	*Date of Uninstallation*
EK12	38.1287	–83.1042	T40/Taurus	vault	yes	09/30/2015	
EK13	38.2301	–82.8286	T40/Taurus	vault	yes	10/18/2015	
EK14	38.2996	–82.7037	TC-PH2/ Centaur	PVC	yes	06/03/2015	
EK20	37.7332	–83.8661	T40/Taurus	vault	yes	11/06/2015	
EK21	37.8160	–83.5315	MC-PH1	PVC	yes	09/02/2015	
EK22	37.9152	–83.2508	MC-PH1	PVC	yes	08/25/2015	
EK23	37.9213	–82.9004	T40/Taurus	vault	yes	09/29/2015	
EK25	38.1359	–82.8145	TC-PH2/ Centaur	direct burial	yes	06/10/2016	
EK26	38.0704	–82.5810	TC-PH2/ Centaur	PVC	yes	06/04/2015	
EK26A	38.0682	–82.5662	T40/Taurus	direct burial	no	10/17/2017	12/05/2017
EK32	37.6198	–83.3024	MC-PH1	PVC	yes	09/02/2015	
EK33	37.7582	–83.1249	T40/Taurus	vault	yes	11/04/2015	
EK34	37.7056	–82.7496	T40/Taurus	vault	yes	06/06/2016	
EK35	37.8569	–82.7147	TC-PH2/ Centaur	direct burial	yes	06/09/2015	
EK36	38.0154	–82.6150	Titan/Taurus	vault	yes	01/20/2017	
EK36A	38.0163	–82.6204	T40/Taurus	direct burial	no	02/03/2017	03/16/2017

details of which are presented in Holcomb (2017). Acquisition parameters and frequency responses to ground motions for the instrumentation deployment are given in Table 5.

Typically, data from all telemetered stations were received at KGS for near-real-time event detection. Occasional cellular-network outages prevented the simultaneous acquisition of all stations' data, however. These communication outages and occasional instrumentation problems resulted in temporary reductions in the sensitivity of the network for real-time analysis. Figure 7 shows the history of telemetry outages through Feb. 21, 2018, and the percentage of the operational lifespan (not including times when the station was malfunctioning) when the streaming data arrived at least five minutes late at KGS. As discussed below, data received five minutes late or later were not included in event triggering.

All stations recorded data locally, and the recordings that were downloaded during site visits were archived at KGS as a continuous data set. These data could be examined in a future, more complete assessment of the seismicity.

Data Acquisition and Analysis

Telemetered waveforms were acquired and processed in near real time on a server at KGS using the Earthworm software package (Johnson and others, 1995 [www.isti.com/products/earthworm; last accessed 02/21/2018]) and events were detected by two different processes: coincidence triggering and grid-based arrival-time association. Detected events were separated into the categories of probable local blasts and local, regional, or teleseismic earthquakes, by manual inspection. Phase arrivals from local earthquakes were picked and events were located using SEISAN analysis software (Havskov and Ottemöller, 1999).

Seismic-Event Detection. Seismic events were detected using telemetered, streaming data from the microseismic monitoring network stations (Table 4) and other nearby stations listed in Tables 2 and 3. Transient signals at individual stations were detected using short-term-average to long-term-average ratios (STA/LTA) of the streaming, bandpass-filtered waveforms (Withers and others, 1998). Events were detected using two methods that are implemented in Earthworm software modules. The first, which was initiated with the deployment of the first monitoring-network station, uses coincidence triggering of station detections; the second uses a gridded-earth model to associate station detections. Both methods detect seismic events—earthquakes and blasts—at local to global scales.

All events detected were registered into a SEISAN database, manually inspected, and categorized. Seismic events, or events detected from seismic-wave arrivals, and not just recordings of correlated local noise, were categorized as either local, regional, or teleseismic based on their proximity to the closest monitoring-network station: Local events were within 250 km, regional events were from 250 to 2,000 km away, and teleseismic events were at distances greater than 2,000 km. The local events were further categorized as either earthquakes or probable mine or quarry blasts, based on waveform characteristics (Holcomb, 2017).

Coincidence Triggering. A coincidence trigger occurs when multiple STA/LTA station detections

Table 5. Eastern Kentucky Microseismic Monitoring Project instrument (originally installed; see Table 4) and acquisition parameters. See Table 4 for original instrumentation. Response type is the type of ground motion to which the instrument responds (m/s for ground velocity; m/s^2 for ground acceleration).Corner period and f_{max} define the long-period and high-frequency boundaries for the seismometers' constant responses to input ground motion, respectively. Sensitivity is the system response to input ground motion, in counts per corresponding ground-motion units.

Instrument	*Data Logger Samples per Second*	*Response Type*	*Corner Period (s)*	*f_{max} (Hz)*	*Sensitivity*
T40/Taurus	100	m/s	40.2	85.5	1.55300×10^9 C s/m
TC-PH2/Centaur	200	m/s	120.2	108	3.01720×10^8 C s/m
MC-PH1	200	m/s	120.2	108	3.00000×10^8 C s/m
Titan/Taurus	200	m/s^2	N/A	430	3.26399×10^6 C s^2/m

Figure 7. Data telemetry latency from June 2015 through January 2018. Blue vertical lines mark instances when streaming data were not received at KGS within five minutes of production. Inset labels are station name and the percentage of the station's operational time when data were not received, or arrived with latency of five minutes or more.

are observed within a specified time window. For this project, Earthworm's CARLSTATRIG calculated the station detections and the CARLSUBTRIG module was used for coincidence-triggering event detection. Prior to calculating station detections with CARLSTATRIG, broadband waveforms were filtered with a passband of 1 to 20 Hz; waveforms from short-period stations were not filtered. For event detection, or network triggering, CARLSUBTRIG was configured to use different subsets of the monitoring network and existing seismic stations to form subnetworks. Figure 8 is an example of one of the subnetwork configurations used during network operation. In the configuration shown, CARLSUBTRIG used three subnetworks, any one of which could detect an event.

Earthworm was configured to declare an event when detections from five stations in the largest subnetwork (yellow-highlighted stations in Figure 8) were recorded within a time window of 35 s, depending on the station; the other two subnetworks shown required four stations to trigger within the same time window. The 35-s time window corresponds to the traveltime of a shear wave from a surface-focus seismic event at a distance of approximately 123 km, which is the maximum separation between monitoring network stations (the distance between EK20 and EK14). The subnetwork configuration was modified as nearby stations were uninstalled (e.g., temporary EarthScope stations) or new network stations were installed.

Using multiple subnetworks reduces the chances of an earthquake not being detected because of station or telemetry outages, or because of high transient-noise levels. To further mitigate reduced detection sensitivity from temporary telemetry outages, coincidence-triggering processing was delayed by five minutes to allow late-arriving station triggers to be a part of the network triggering.

Grid-Based Station-Detection Association: BINDER. STA/LTA station triggers were also analyzed by Earthworm's grid-associator, BINDER. BINDER attempts to identify sets of station triggers that are consistent with the theoretical traveltimes of P- and S-wave arrivals for local seismic events. Theoretical traveltimes were calculated using an earth model appropriate for the region—the HAMBURG model (Herrmann and Ammon, 1997) was used for this project—and a grid of candidate source locations, with 4.0-km spacing between nodes. When the trigger times from at least four stations are consistent within approximately 2.0 s on average of the predicted traveltimes from a particular grid node (calculated as the root-mean-square residual), BINDER declares an event. Prior to calculating station triggers for event detection with BINDER, broadband waveforms were filtered with a passband of 4 to 20 Hz, which is necessary to extract signal through lower- and higher-frequency noise.

Seismic-Event Analysis. For all local earthquakes, first-arrival body waves were manually picked; P-wave arrivals were picked on vertical-component recordings and S-wave arrivals on transverse, horizontal components. Events were located using the Gauss-Newton algorithm HYPOCENTER (Lienert and Havskov, 1995) in SEISAN, which is discussed more fully in Holcomb (2017). The location inversion was configured to account for arrival weights based on analyst-estimated arrival-time measurement uncertainties and event-station offsets, and a regional velocity model was used to calculate the predicted first-arrival traveltimes and the partial-derivative matrix. Table 6 shows the weighting scheme that was used to down-weight phase arrival picks based on their arrival-time uncertainties. The distance weighting scheme used further decreased arrival weights from full weight from 1.0 at 0 km offset to zero weight at 250 km offset. Figure 9 shows the velocity structure(s) used in this study: the HAMBURG model and the model developed by Chapman and others (1997) for the Eastern Tennessee Seismic Zone. Both models were tested for each event location, and the model producing the lowest root-mean-square arrival-time residuals was used to determine the final hypocenter.

The appropriateness of the velocity models used in this study area is demonstrated in Figures 10 and 11. Figure 10 shows the traveltime residuals (observed minus predicted traveltime) from all earthquakes within the project area. The residuals reflect the accuracy of the manually determined arrival-time picks and the accuracy of the velocity model used. The scatter of the residuals increases with distance, which is expected because of reduced signal quality with distance as a

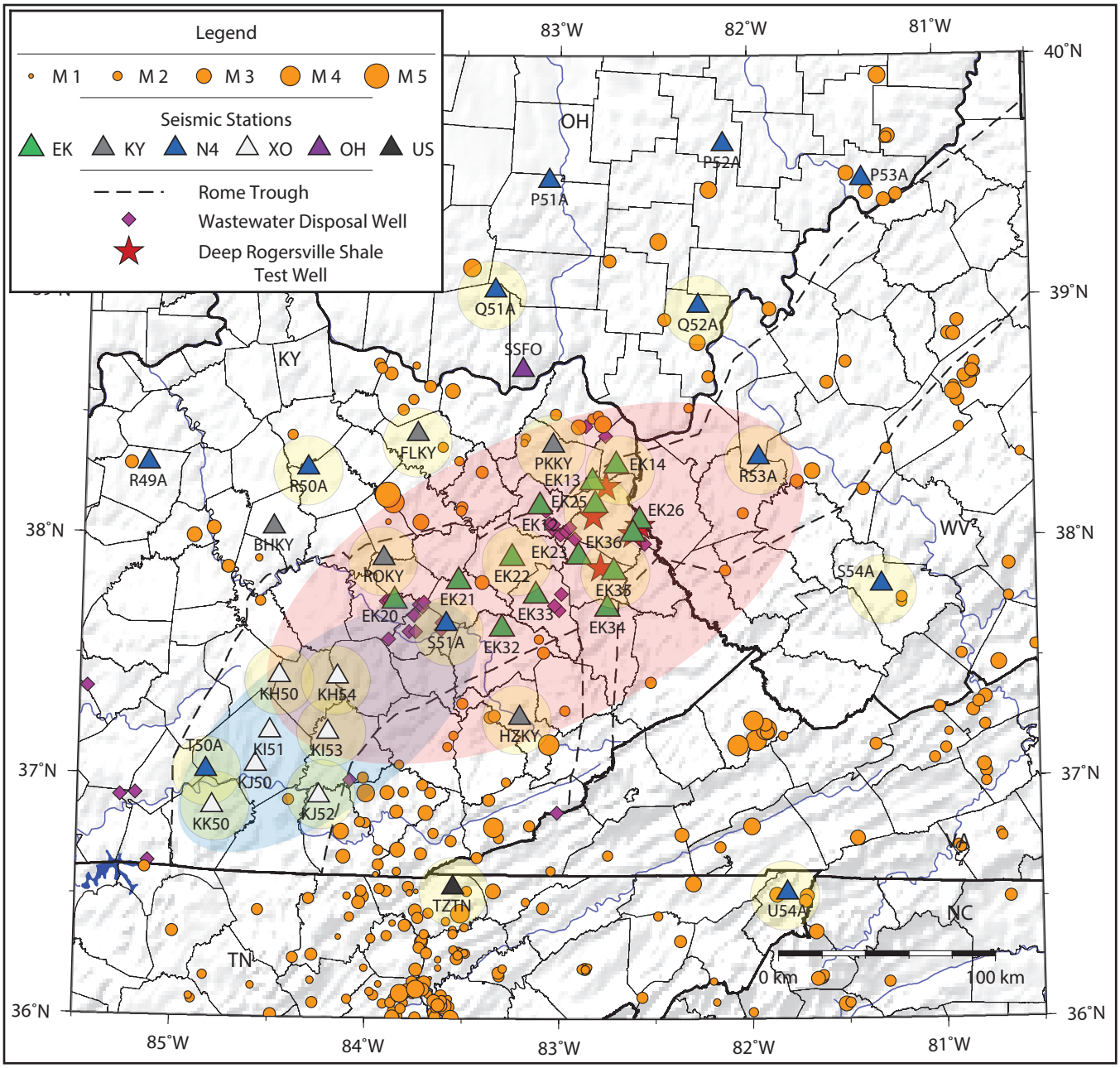

Figure 8. One of three subnetwork configurations used for coincidence triggering to detect seismic events. The subnetworks, or groups of stations that can be triggered within a defined time window, used in the configuration shown are highlighted in blue, pink, or yellow. Other symbols are as in Figure 4.

result of attenuation effects along the travel path. This results in increased uncertainties, or errors, in the arrival-time picks with distance. The lack of a systematic offset or trend in the residuals with distance, indicated by the best-fitting line through the residuals, shows that the velocity structures used for the locations are appropriate. The location of a known cooling-tower collapse and its location determined using the P-waves recorded by monitoring network stations (the closest station was 12 km away) using the HAMBURG velocity model are compared in Figure 11. The calculated location, less than 300 m to the north, is very close to the tower, which further supports the appropriateness of this velocity model for the project area.

Magnitudes were calculated for all located events using both an amplitude-based scale (M_L) and a signal-duration-based scale (M_c). Duration

Table 6. Arrival-time-pick uncertainties (code assigned by analyst while picking arrival times) and corresponding weights (assigned by HYPOCENTER for the arrival-time inversion) for event-location calculations.

Code	*Uncertainty (s)*	*Weight*
0	≤0.075	1
1	≤0.15	0.75
2	≤0.225	0.5
3	≤0.3	0.25
4	>0.3	0

magnitude is determined from the coda length, or length of time from the arrival of the P-wave to when the signal amplitudes decay to background-noise levels. Duration magnitudes are routinely reported by regional networks in the eastern United States and are the standard magnitude type for low-magnitude events. Therefore, the M_C scale was used for events located in this study when possible.

Duration magnitudes were estimated using the relationship of Chapman and others (2002):

$$M_C = -3.45 + 2.85\ log_{10}(D) \quad (1)$$

where D is the coda length in seconds. The median of the individual station values is reported for the event.

The local magnitude scale (M_L) is determined from amplitude measurements, and is analogous to the Richter magnitude scale developed for California (Richter, 1935). M_L is calculated from the manually measured, maximum zero-to-peak amplitudes on all horizontal-component waveforms with discernable S-wave or Lg-wave arrivals. Prior to measuring amplitudes, we corrected the waveforms for the effects of the corresponding recording instruments (Table 5), integrated to displacement, and then bandpass-filtered, following the procedure of Alsaker and others (1991), to simulate the recordings of a Wood-Anderson seismometer, which was used by Richter (1935). The coefficients, which account for the S-wave and Lg-wave attenuation in the region, were calibrated by an inversion algorithm in SEISAN so that an M_L 3.0 earthquake produces a displacement of 1 mm at 100 km offset, consistent with Richter's scale. Station-correction terms were also derived as part of the procedure, which accounts for any systematic biases from site effects or unmodeled instrument responses.

The local magnitude scale is less susceptible to changes in local site noise—for example, from ostensible seasonal variations and from diurnal variations from manmade sources—and therefore should provide a more consistent measurement of magnitude than the duration-magnitude scale. Furthermore, preliminary findings in Holcomb (2017) suggest that local magnitudes from the monitoring network are more consistent with the energy-based moment-magnitude scale than duration magnitudes. Thus, an M_L relationship was derived for the microseismic monitoring network, and is given in the **Results** section.

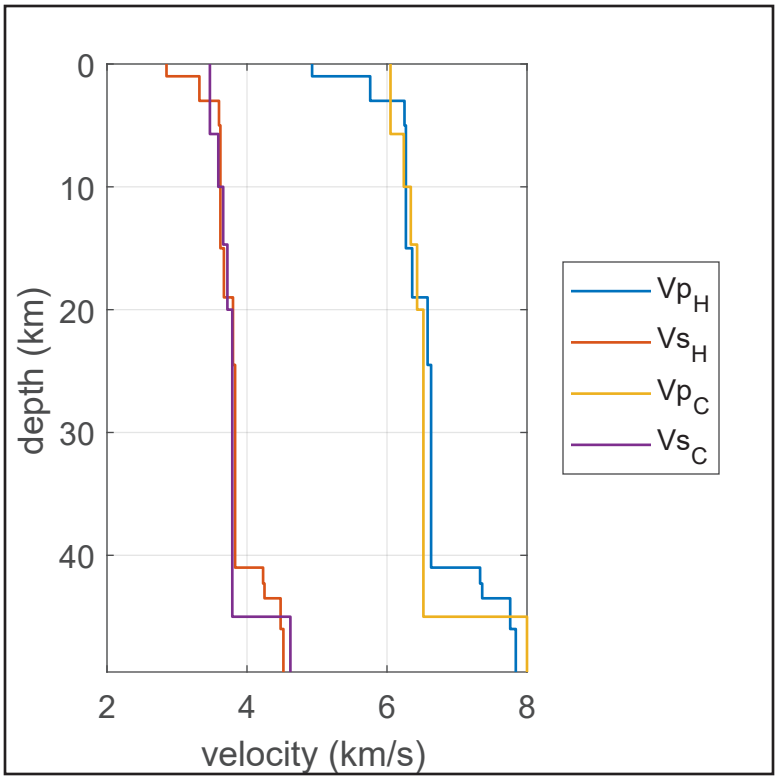

Figure 9. Velocity models used to determine earthquake locations. Vp is P-wave velocity; Vs is S-wave velocity. H and C subscripts correspond to the modified HAMBURG (Herrmann and Ammon, 1997) and Chapman and others (1997) velocity models, respectively. The HAMBURG model was modified to remove low-velocity zones for use with the HYPOCENTER program.

Detection-Threshold Modeling

Site noise, which commonly arises from cultural sources, is a frequency-dependent limiting factor of station sensitivities to weak events. To assess site noise lev-

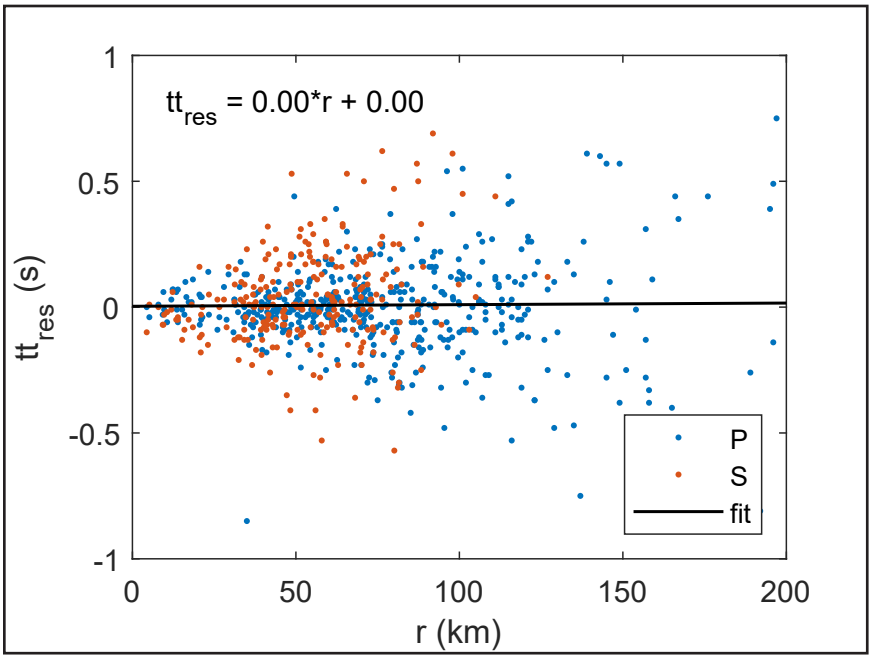

Figure 10. P- and S-wave traveltime residuals versus hypocentral distance for all events in the project area. The equation of the best-fitting line through these residuals is shown. Although the magnitude of the residuals increases with distance, the fact that the average residual is zero to two significant digits regardless of distance indicates that the velocity models used are appropriate and do not systematically bias the traveltime predictions.

els, Holcomb (2017) developed probabilistic noise models for one month of the microseismic monitoring network's and regional stations' recordings during evening and daytime hours using the PQLX software package and methodology described in McNamara and Boaz (2011). Figure 12 shows example noise models for two stations. For this project, the median noise models were used to model the event-detection threshold, or the minimum-magnitude earthquake detectable in the project area. These detection-threshold maps estimate the sensitivity of the seismic network and are valuable in regions such as the project area, where seismicity rates are low and recurrence relationships based on observations (e.g., Gutenberg-Richter curves) have large uncertainties.

Holcomb (2017) used the median noise models at each station and theoretical earthquake amplitude spectra, *A(f)* (equation 2), to model the minimum-magnitude earthquake detectable by the stations used for event triggering (Fig. 8, Tables 2–3):

$$A(f) = S(f) \times D(f) \times G(R) \qquad (2)$$

Theoretical amplitude spectra are the product of earthquake source spectra, *S(f)*, a diminution function, *D(f)*, which accounts for intrinsic energy loss, and a geometrical spreading function *G(R)*. The source spectra were simulated using the Boatwright (1980) source model, and parameter values used in the *D(f)* and *G(R)* attenuation expressions were determined for eastern North America by Atkinson and Boore (2014) and Herrmann (1983), respectively.

Amplitude spectra were calculated at 5-km intervals across the local area in a regular grid and at depths of 4.0 km, corresponding to the approximate basement depth beneath the Rogersville Shale, and for moment magnitudes ranging from 0.2 to 1.8, in increments of 0.1 magnitude units. A station detection occurred when the ratio of the theoretical spectrum to the corresponding station's noise spectrum, or the pseudo-theoretical signal-to-noise ratio, exceeded 3.5, corresponding to the signal-to-noise threshold ratio used for event detection. The smallest magnitude at which at least four pseudo-theoretical station detections occurred at a given node was then the minimum detectable event for that node. This process was conducted for both daytime and nighttime noise models to produce detection-threshold maps for the project area for typical noisy (daytime) and quiet (nighttime) conditions, assuming all stations and network communications were functional.

Results and Discussion

As of the time this report was being written, the microseismic monitoring network continues to operate and analysis of its recordings is ongoing. The following results and discussion are based on the analysis of the network recordings completed at that time.

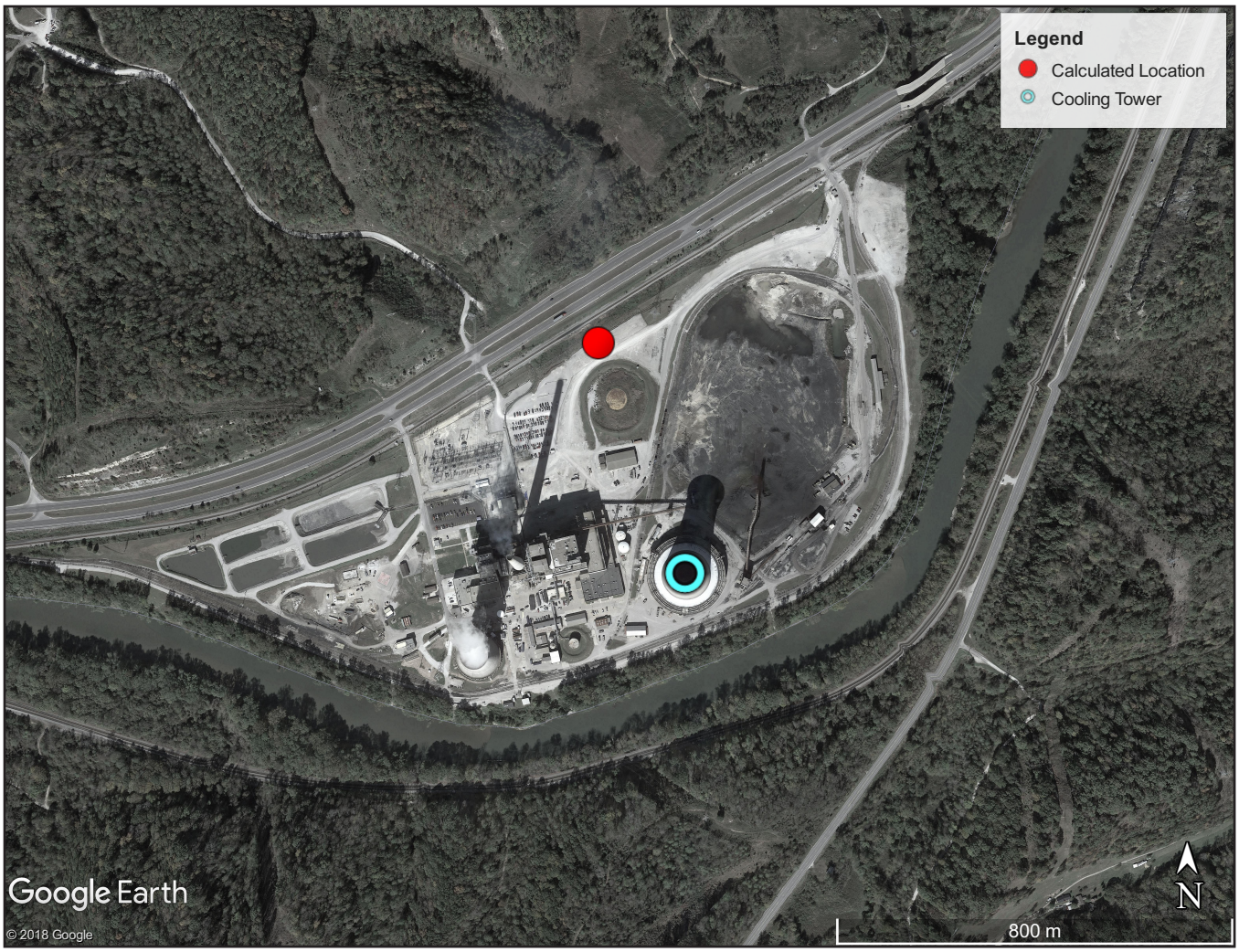

Figure 11. Ground-truth evaluation of the location accuracy using seismic waves induced by a cooling-tower demolition in the project area (12 km from the closest station). The cooling tower's location is shown by satellite imagery taken prior to the demolition and the location determined using P-waves recorded by the microseismic monitoring network stations is shown in red, approximately 300 m to the north-northwest. Satellite image ©2018 Google.

Monitoring-Network Data Set and Telemetry Latency

The monitoring network has generated a large waveform data set, which is the primary component used for this project. Successful operation of the network and acquired recordings have allowed background seismicity to be cataloged for the project area, including a calibrated magnitude scale, discussed below. Figures 13 and 14 are example recordings. Figure 13 shows typical seismograms from an earthquake within the project area. This particular example is from an M_L 1.4 earthquake within the Rome Trough of eastern Kentucky. The earthquake produced high-quality recordings on the monitoring network and several regional stations, but was undetected by routine, regional monitoring event-detection algorithms. Figure 14 shows four days of waveforms and spectrograms from the two stations operating nearest to and during the hydraulic fracturing of the Walbridge Holdings LLC well, which was completed in the Rogersville Shale. Ten stages of the completion, which produced ground motions (either from subsurface or surface activity) that are clearly evident in these recordings, are shown.

The number of hour-long, continuous data files recorded by the monitoring network and the total volume of the data at the time this report was prepared are given in Table 7. The recordings are in miniSEED format and stored on servers at KGS.

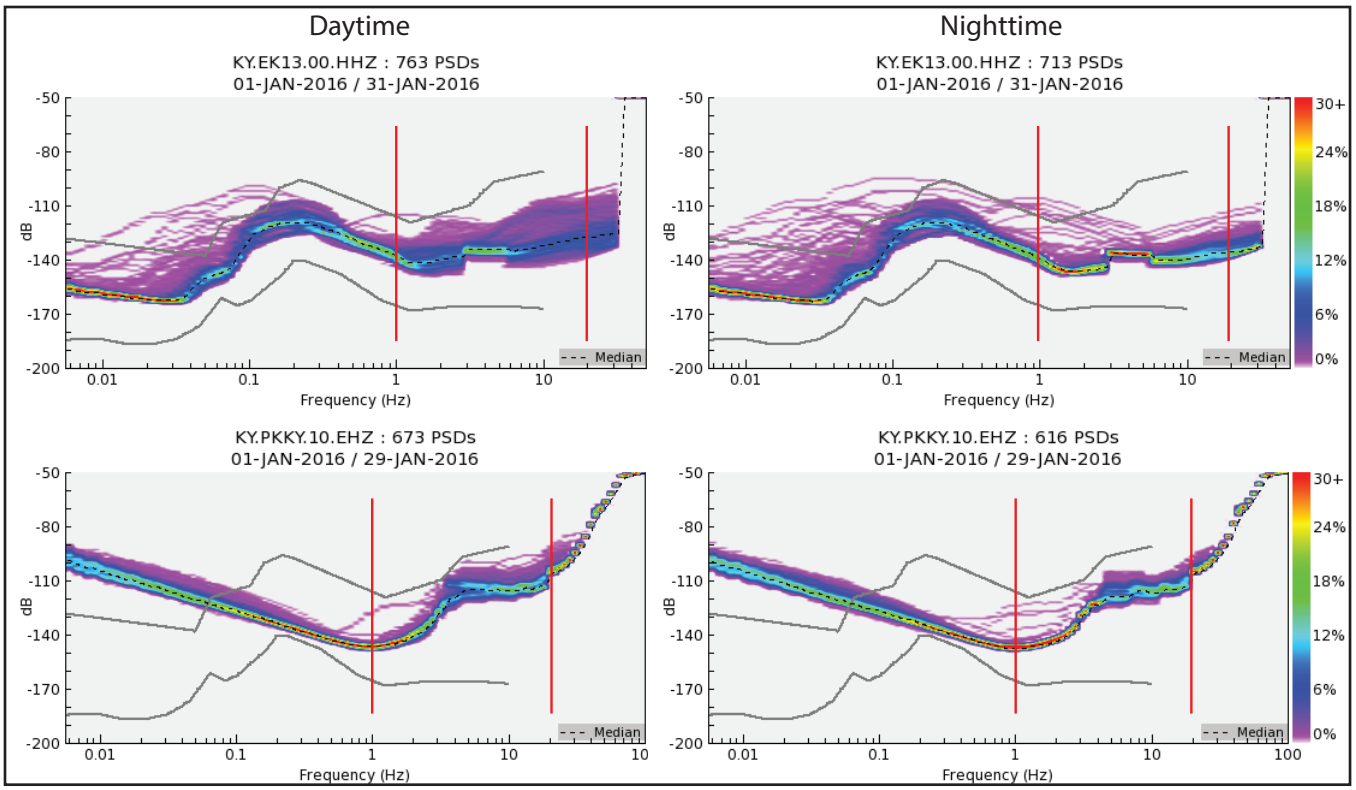

Figure 12. Noise models developed for a broadband station (EK13; top row) and a short-period station (PKKY; bottom row) for daytime hours (left column) and nighttime hours (right column), colored by probability; median values are black, dashed curves. Black curves are global average high (generally above the station median noise level) and low (generally below) noise levels. Red lines bound the frequency band of local earthquake detection.

Table 7 also includes an estimate of the real-time data completeness (Fig. 7) in terms of the percentage of the operational lifespan of a monitoring network station that the streaming recordings were not available for event triggering. This is a minimum estimate, and does not account for stations or telemetry links that were down for more than five days. The percentage of time since installation that the major components of the station (seismometer and data logger) operated properly is also shown in Table 7. Both of these factors affect the performance of the monitoring network by temporarily decreasing its sensitivity.

Magnitude Scales and Attenuation

Two scales were used to determine the magnitudes of the earthquakes listed in Table 8: coda (equation 1), M_C, and local, M_L. Using the SEISAN inversion scheme previously discussed, a calibrated M_L scale was developed for the monitoring network:

$$M_L = log_{10}(A) + 1.1198\ log_{10}(r) + 0.00025r - 1.9467 + s \quad (3)$$

where A is the displacement amplitude (zero-to-peak) in nanometers, measured on a Wood-Anderson simulated seismogram, r is the hypocentral distance in kilometers, and s is the station-specific correction term. The final result, event M_L, is the median value of the horizontal-component magnitudes determined with equation 3. The terms in equation 3 that account for regional attenuation from geometric spreading and heat loss, and a static correction, are:

$$-log_{10}(A) = 1.1198\ log_{10}(r) + 0.00025\,r - 1.9467. \quad (4)$$

This expression, known as the attenuation correction, can be compared with other attenuation correction functions derived for the region shown in Figure 15. The similarity between equation 4 and the attenuation-correction functions determined for other stable continental regions—K98 (eastern North America) and Nor (Norway)—shows that equation 4 and therefore the M_L scale in equation 3 are reasonable.

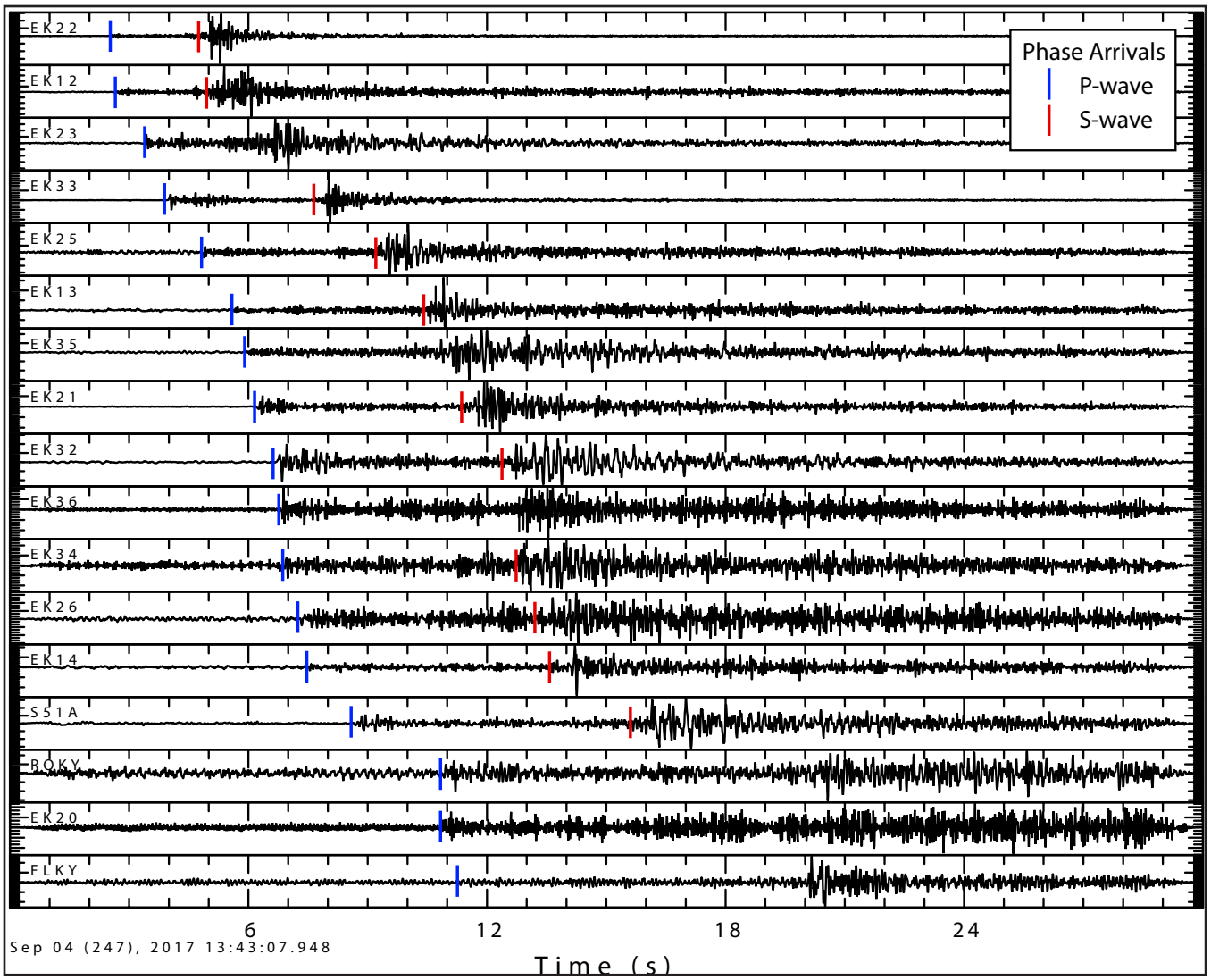

Figure 13. Microseismic network and regional network seismograms from an M_L 1.4 earthquake within the Rome Trough of eastern Kentucky recorded at distances from 15 to 73 km from the hypocenter. The onsets of identifiable P- and S-phase arrivals are indicated with blue and red vertical lines, respectively.

Preliminary findings in Holcomb (2017) that suggested that local magnitudes in the monitoring network are more consistent with the energy-based moment-magnitude scale than duration magnitudes, which show a bias toward larger values, motivated development of an M_L scale for the project area. A comparison between local and coda magnitudes in the monitoring-network catalog shown in Figure 16 demonstrates that M_c is systematically larger than M_L, which was also observed from coda magnitudes in the Advanced National Seismic System Comprehensive Earthquake Catalog. The monitoring network and ANSS Comprehensive Catalog coda magnitudes were evaluated using Gutenberg-Richter magnitude-frequency curves (discussed in the following section), which revealed anomalous relationships between the coda magnitudes and the annual frequencies of occurrences. In contrast, the local magnitudes subjected to the same analysis were consistent with global observations. For these reasons, M_L is the preferred magnitude for our monitoring-network catalog.

M_L residuals, calculated as the event M_L minus the single-observation M_L, are plotted versus hypocentral distance in Figure 17. The scatter was expected, largely because of intra-event differences from earthquake radiation patterns, but the long wavelength oscillations, uncorrected by this linear scale, indicate that the actual attenuation is more

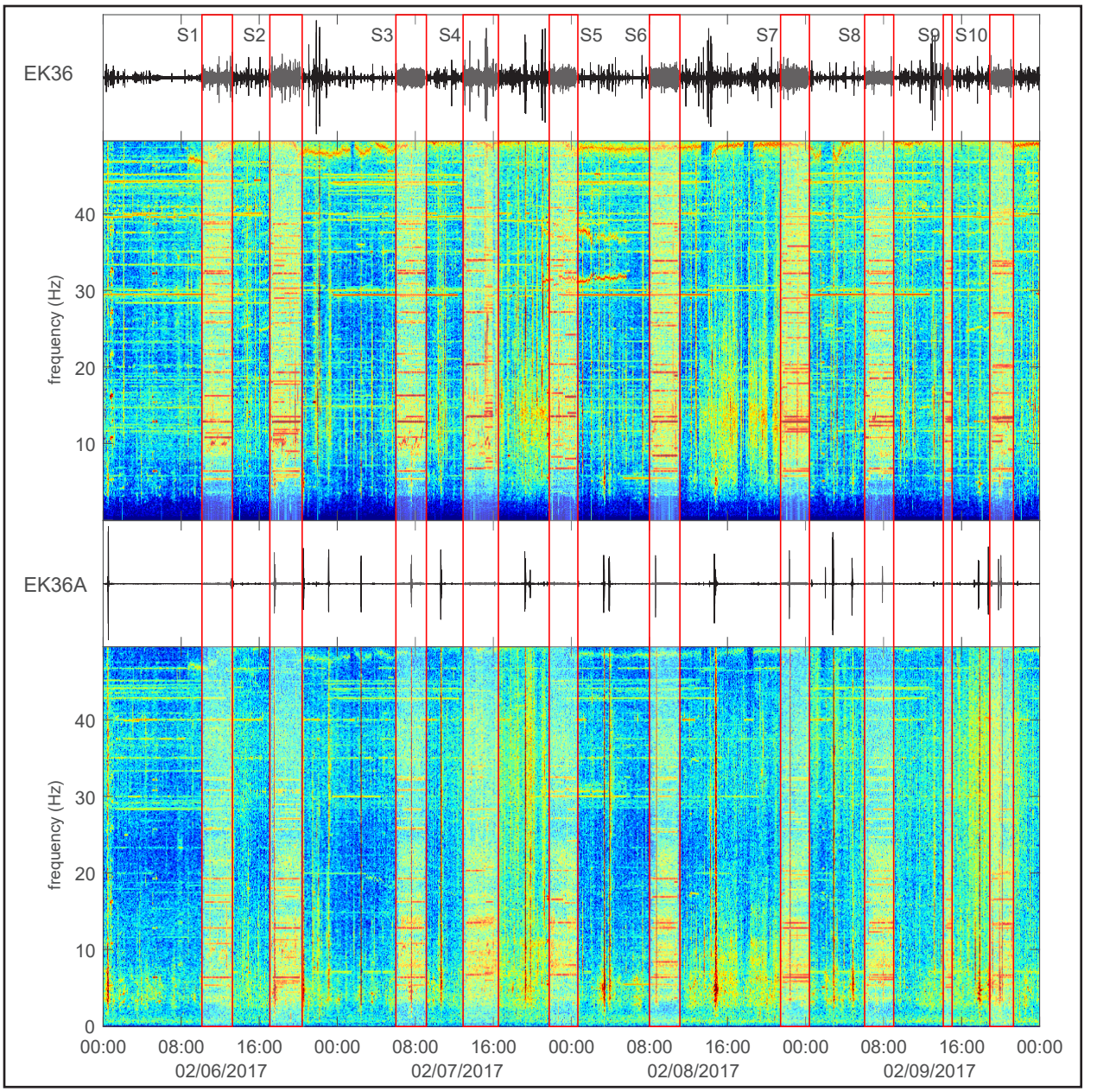

Figure 14. Four days of continuous waveforms, labeled by station name, and the corresponding spectrograms (the distribution of amplitudes across frequencies from 0 to 50 Hz versus time) during 10 stages of the hydraulic fracture stimulation of the Walbridge Holdings LLC test well, labeled S1 through S10. Plots use relative scaling; warmer colors show larger amplitudes. EK36 and EK36A were 210 m and 640 m, respectively, from the wellhead.

complicated than a simple linear model. Because the median of the station magnitudes is reported as the event magnitude, however, systematic biases in the local magnitudes are not expected.

The complexity of the regional shear-wave attenuation has been noted in other studies in the eastern United States (e.g., Burger and others, 1987). In particular, an increase in the amplitudes of shear waves creates a larger ground motion at the surface at distances consistent with the increasing residuals, from approximately 80 to approximately 200 km, shown in Figure 17. This increase has been attributed to the post-critical shear-wave reflections off the Moho, and the observations of this phenomenon in eastern Kentucky indicate that ground-motion attenuation models should account for this effect for seismic-hazard assessment.

Table 7. Eastern Kentucky Microseismic Monitoring Project data set, station operational periods, and telemetry latencies as of 06/05/2018. N = number of hour-long miniSEED data files recorded (dependent on the most recent on-site data download, and will not be the final number of files for the project). Size = total size of the data volume for this station (dependent on the most recent on-site data download, and will not be the final amount of data for the project). Lifespan = the number of days the station operated through 06/06/2018. Operational percentage = the percentage of the lifespan during which the station's data logger and seismometer functioned properly through 06/06/2018. Latency = the estimated percentage of a station's lifespan that data streams were not available, or latent for greater than five minutes through 06/06/2018 (a dash indicates a nontelemetered station).

Station	*N*	*Size (GB)*	*Lifespan (days)*	*Operational Percentage*	*Latency (%)*
EK12	53,655	31.3	949	95.9	0.83
EK13	64,004	29.8	960	88.9	0.88
EK14	74,643	66.8	1,098	99.2	0.33
EK20	56,259	29.0	942	98.4	1.29
EK21	62,354	99.5	1,007	91.8	1.06
EK22	64,089	101.2	1,015	99.7	1.33
EK23	63,351	45.8	950	99.7	9.2
EK25	73,449	65.9	1,091	99.0	10.17
EK26	73,887	70.4	1,097	100.0	0.80
EK26A	3,522	4.2	48	100.0	–
EK32	65,421	104.2	1,007	97.4	4.85
EK33	62,679	32.8	944	100.0	1.98
EK34	47,154	29.1	729	98.1	0.72
EK35	73,398	65.9	1,092	99.8	3.87
EK36	30,975	35.9	501	100.0	0.93
EK36A	2,934	3.3	39	100.0	–

Seismicity

The monitoring network and contributing regional stations detected 47,237 events by coincidence triggering from June 11, 2015, through May 31, 2018. A total of 28,793, or 61 percent, of the triggers were identified as seismic events; the remainder were triggered by noise sources (e.g., local cultural noise or thunderstorms). A total of 25,771 triggers from local mine blasts were recorded, which constitute almost 90 percent of the seismic events. Of the remaining triggers, 1,679 were from teleseismic earthquakes and 1,191 were from regional events. Less than 1 percent of the seismic events (151) were from local earthquakes. The BINDER method, which was initiated on April 12, 2016, detected more than 6,700 events through May 31, 2018; 79 local earthquakes were located by this method.

The seismicity illustrated in Figure 18 (Table 8) includes the 38 local earthquakes detected by either real-time method, and located in the project area. There are fewer earthquakes (13) in the Advanced National Seismic System event catalog in the same region (Fig. 18), for the same period. The earthquake locations in the ANSS catalog are generally similar to the corresponding event locations determined for this study. It is notable, however, that none of the six earthquakes detected by our microseismic monitoring network stations within the Rome Trough of eastern Kentucky were included in the ANSS Comprehensive Earthquake Catalog.

The earthquake focal depths were consistent with seismicity in the local area (Carpenter and others, 2014), with most earthquakes occurring at depths shallower than 25 km below sea level (Fig. 19). Numerous shallow-focal-depth earthquakes were recorded, occurring primarily in southeastern Ohio, near the border with West Virginia. Furthermore, the spatial distribution of the seismicity observed by the monitoring network is consistent with the long-term seismicity catalog for

Table 8. Local earthquake source and location-quality parameters. Depth is with respect to sea level. M_L is from equation 3. M_c is from equation 1. RMS = root mean square of the arrival-time residuals for the reported location. N_{pha} = number of phases used to determine the hypocenter. Gap = the largest azimuthal separation between stations used to determine the hypocenter. D_{min} = distance to the closest station used to determine the hypocenter. E_{lon} = standard error in longitude. E_{lat} = standard error in latitude. EZ = standard error in depth.

Date	*Time*	*Latitude (°N)*	*Longitude (°E)*	*Depth (km)*	*M_L*	*M_c*	*RMS (s)*	*N_{pha}*	*Gap (°)*	*D_{min} (km)*	*E_{lon} (km)*	*E_{lat} (km)*	*EZ (km)*
06/27/2015	07:16:24.7	38.6407	–82.9005	1.1	0.9	1.2	0.08	9	198	30.9	4.2	4.8	10.3
11/29/2015	01:27:29.8	38.2362	–83.2236	21.9	1.6	2.2	0.12	29	58	15.9	0.7	0.9	1.4
12/13/2015	00:41:17.6	38.6700	–83.9899	10.0	1.0	1.8	0.08	8	200	34.2	1.9	2.7	12.5
12/22/2015	15:20:32.9	38.2618	–83.4182	0.8	1.5	1.7	0.13	30	64	31.2	0.8	0.6	1.8
02/02/2016	08:09:02.4	38.3312	–84.3929	34.4	1.2	1.3	0.09	13	173	8.0	1.8	1.3	1.6
02/24/2016	03:30:05.0	38.5290	–83.8416	5.0	1.4	1.8	0.16	21	161	13.9	1.2	1.3	3.8
04/26/2016	19:24:03.8	38.1238	–83.5103	5.0	1.6	2.0	0.13	26	47	32.5	0.6	0.7	2.5
08/06/2016	12:39:13.8	37.8899	–82.0948	34.2	2.0	2.2	0.23	31	84	47.2	1.3	1.0	2.8
09/20/2016	11:10:52.9	37.6745	–82.7800	20.4	1.4	1.7	0.16	23	171	4.4	1.3	1.6	1.6
09/22/2016	12:57:21.6	37.3886	–82.5313	28.8	1.8	2.4	0.18	32	80	40.1	1.0	2.0	2.6
10/17/2016	10:14:17.4	37.6743	–82.2233	17.5	1.2	1.7	0.19	25	187	46.5	1.6	1.5	5.9
12/03/2016	16:54:19.1	37.7328	–84.2931	37.7	0.9	0.9	0.07	12	120	37.6	3.4	3.2	4.4
12/10/2016	22:19:08.9	38.2826	–83.3367	3.1	0.9	1.3	0.05	10	196	26.6	1.8	1.6	4.0
12/22/2016	04:34:26.4	38.4123	–83.1857	21.1	1.2	1.7	0.08	21	77	13.6	1.0	1.2	3.1
01/03/2017	11:25:17.5	38.1715	–83.3033	11.7	0.4	0.5	0.12	17	99	18.1	1.2	1.8	3.4
01/23/2017	06:30:23.3	38.5388	–82.3190	29.3	1.5	2.0	0.13	24	89	39.5	0.8	1.3	3.2
01/25/2017	22:54:10.4	38.6553	–83.3081	18.6	1.4	1.9	0.13	22	110	38.5	0.7	1.3	2.1
02/20/2017	03:49:37.2	37.9676	–82.5286	10.4	0.4	1.1	0.16	19	236	9.3	1.1	2.0	1.7
02/22/2017	09:44:36.7	37.2125	–82.8404	17.2	1.2	2.2	0.14	22	121	32.8	0.9	1.8	3.0
03/04/2017	12:43:17.9	38.4951	–83.0221	21.0	1.6	2.6	0.09	23	225	12.5	3.1	2.3	3.8
03/26/2017	17:56:13.9	38.1194	–83.3006	19.5	0.5	0.4	0.14	12	222	17.2	2.3	3.0	3.6
06/20/2017	02:06:48.3	37.2513	–83.3409	7.5	2.1	2.9	0.20	27	100	11.9	1.3	1.8	4.0
07/18/2017	22:52:20.5	38.4570	–83.2152	5.0	1.1	1.5	0.04	12	270	37.7	3.2	3.1	20.3
07/19/2017	01:23:12.4	38.4524	–83.2012	10.3	0.7	1.0	0.05	10	287	16.5	3.1	3.0	13.4
08/24/2017	05:56:10.4	37.9924	–84.0773	9.8	0.9	1.2	0.12	13	244	16.2	1.4	3.0	5.4
09/04/2017	13:43:06.9	37.9930	–83.1262	16.5	1.4	1.7	0.08	32	56	13.9	0.5	0.5	1.1
10/13/2017	07:02:09.6	38.3673	–83.6159	10.2	1.0	1.6	0.12	22	79	13.4	0.9	0.7	2.5
10/16/2017	22:10:15.0	37.9919	–84.4791	16.0	1.5	2.1	0.10	16	102	5.2	0.7	1.3	1.1
10/18/2017	15:54:38.6	37.9992	–84.4748	18.6	1.9	2.5	0.11	21	102	33.9	1.0	1.3	2.0
10/22/2017	01:12:04.9	37.1776	–83.6400	15.2	1.1	1.9	0.12	12	138	51.4	2.8	4.1	11.1
10/23/2017	22:04:07.3	37.5585	–83.2108	16.1	1.1	1.0	0.15	16	217	10.6	1.5	1.3	1.8

Table 8. Local earthquake source and location-quality parameters. Depth is with respect to sea level. M_L is from equation 3. M_c is from equation 1. RMS = root mean square of the arrival-time residuals for the reported location. N_{pha} = number of phases used to determine the hypocenter. Gap = the largest azimuthal separation between stations used to determine the hypocenter. D_{min} = distance to the closest station used to determine the hypocenter. E_{lon} = standard error in longitude. E_{lat} = standard error in latitude. EZ = standard error in depth.

Date	*Time*	*Latitude (°N)*	*Longitude (°E)*	*Depth (km)*	M_L	M_c	*RMS (s)*	N_{pha}	*Gap (°)*	D_{min} *(km)*	E_{lon} *(km)*	E_{lat} *(km)*	*EZ (km)*
11/03/2017	02:18:25.4	38.5672	–83.8631	11.9	0.6	0.9	0.15	12	169	18.5	2.6	1.9	5.9
11/10/2017	14:22:05.7	37.4472	–83.3871	18.4	1.4	1.9	0.11	16	244	20.6	2.1	1.1	1.4
11/11/2017	00:37:08.7	38.4408	–83.6437	8.9	0.9	1.3	0.11	15	122	9.5	0.9	1.6	2.7
12/17/2017	05:08:35.9	38.6806	–83.9025	12.5	2.0	3.5	0.15	28	75	31.2	0.9	1.2	3.5
03/09/2018	16:27:02.1	37.2755	–82.9693	14.9	1.6	1.9	0.18	18	181	21.2	1.5	2.0	4.5
03/25/2018	09:26:49.6	38.6418	–83.4274	15.4	1.2	2.3	0.08	25	113	20.9	0.6	0.7	2.0
04/06/2018	17:34:58.3	37.5528	–82.5526	21.9	1.5	1.8	0.13	20	282	36.6	2.6	2.7	7.3

the region (compare Figures 4 and 18). Earthquakes occur mostly outside of the Rome Trough and are distributed throughout the region, with no obvious lineations. The existence of such lineations, which was proposed by Chapman and others (1997) in the Eastern Tennessee Seismic Zone south of the project area and which might delineate long, seismically active faults, is not necessarily precluded by these observations; a seismicity catalog that spans a longer time is required to investigate their existence.

There is a contrast in seismic activity between the Rome Trough of eastern Kentucky and its surroundings. Even though the monitoring network focused on the Rome Trough, only six earthquakes, or 16 percent of the 38 events observed in the project area, occurred within the trough's bounding faults. This contrast suggests a difference in the seismogenic potential of the Rome Trough compared to the surrounding regions; additional research is required to constrain the cause of the difference. Of these six earthquakes within the Rome Trough of eastern Kentucky, the epicenter of only one was within 5 km of a wastewater-injection well. That M_L 0.4 earthquake occurred on Feb. 20, 2017, and its epicenter is 2.0 km from injection well EPA ID KYS1270202. No injection volumes have been reported since 2007 for this well (Table 1), and the earthquake focal depth, which is well constrained by nearby P- and S-wave arrivals (Fig. 20), of 10.4 ±1.7 km is much deeper than the injection interval, indicating that this event was not induced.

Gutenberg-Richter diagrams of subsets of the seismicity in Table 8 and of the events located by the monitoring network (within 250 km of the network) are shown in Figure 21. The cumulative number of events per year above a given magnitude versus magnitude is plotted on Gutenberg-Richter curves, the linear parts of which are useful to determine recurrence rates. Globally, where seismicity is caused by tectonic stress release through brittle failure on existing faults, the magnitude of the slope of the linear part, the b-value, is approximately 1.0 (Stein and Wysession, 2009). Assuming seismicity is a self-similar, or fractal, process, the minimum magnitude of the linear part of the Gutenberg-Richter curve is considered to represent the low-magnitude limit of a catalog's completeness, or the magnitude above which all earthquakes in the region have been detected.

Only events recorded since the complete monitoring network was in operation (32 events; first event occurred in June 2016) were used to generate the Gutenberg-Richter curves shown in Figure 21. The b-values for the project area and within 250 km of the project area are 1.0 and 1.1, respectively, and are similar to those observed globally. This suggests that tectonic strain is released through earthquake activity in the vicinity of the project area in a self-scaling process, as is the typical case globally. The curves shown in Figure 21 were also used to estimate the magnitude of completeness of the catalog since June 2016, using the

maximum-curvature method (Wiemer and Wyss, 2000): M_L 1.4 in the project area and M_L 1.9 within 250 km of the network. There are not enough events in the catalog to perform separate and robust Gutenberg-Richter analyses for nighttime and daytime hours.

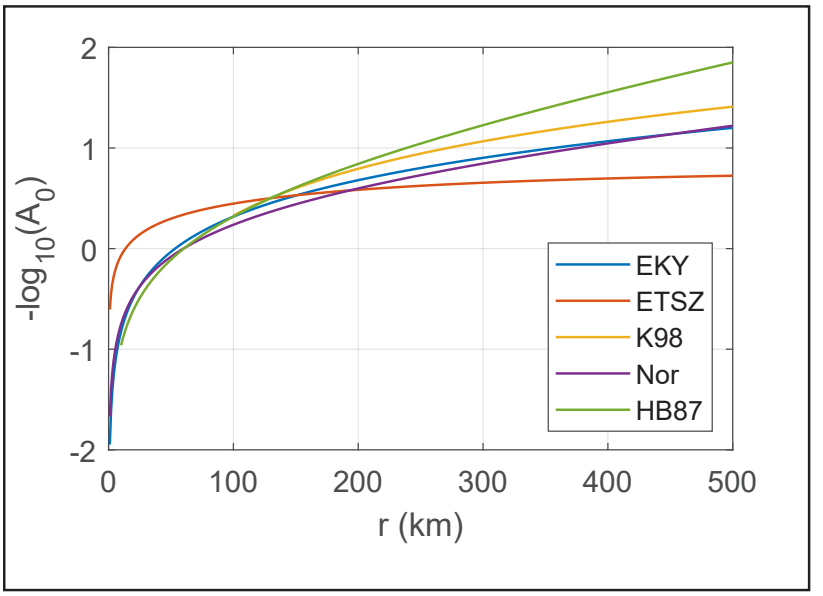

Figure 15. Attenuation correction function derived for the Eastern Kentucky Microseismic Monitoring Project (EKY; equation 4) and those derived in other studies: Eastern Tennessee (ETSZ; Bockholt and others, 2015), just south of the project area, the eastern U.S. (K98; Kim, 1998), Norway (Nor; Alsaker and others, 1991), another stable-continental region, and for California (HB87; Hutton and Boore, 1987).

Regions of variable seismic activity are included in the project area—the active Eastern Tennessee Seismic Zone to the south of the Rome Trough of eastern Kentucky, the active region to the north of the Rome Trough, and the relatively inactive Rome Trough itself—and thus events from regions with different seismicity rates (ordinates of the Gutenberg-Richter plots) were included in the monitoring-project event catalog. There are too few events in the project area to analyze these regions with separate Gutenberg-Richter plots, however, and therefore the curves reveal an area-weighted average of the b-values, seismicity rates, and catalog completeness estimations across these regions. The other important factors that affect the catalog completeness estimate are differences in network sensitivity due to variations in the site-noise levels between day- and nighttime hours and occasional station and telemetry outages.

Although the monitoring network was capable of recording very low-magnitude earthquakes in the project area, as described in the next section, the actual network sensitivity is not reflected by the monitoring project catalog magnitude of completeness.

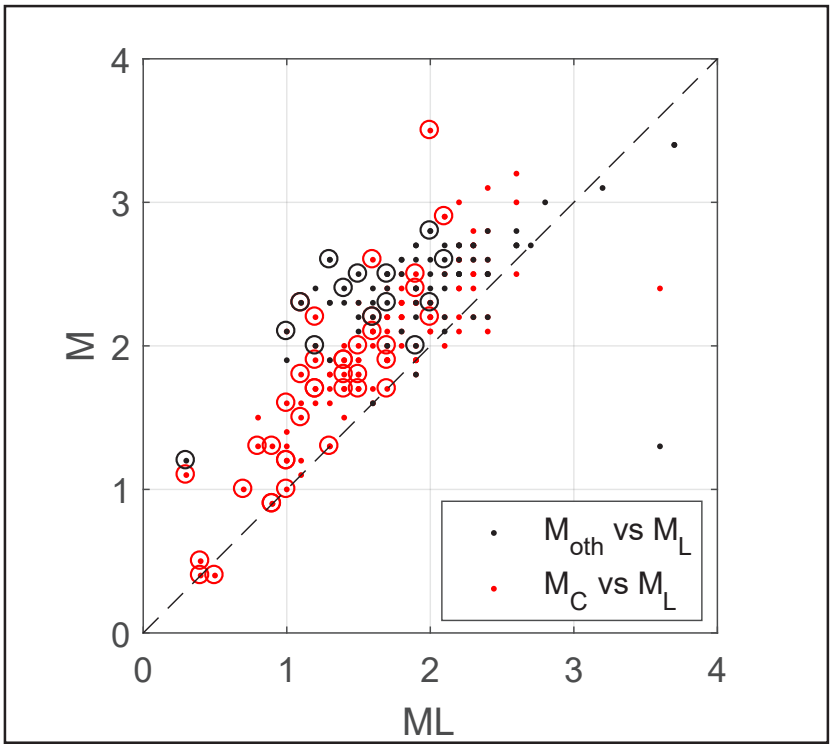

Figure 16. Comparison of M_L with M_C magnitudes from the Eastern Kentucky Microseismic Monitoring Project (red) and M_L from the microseismic project with magnitudes from the Advanced National Seismic System Comprehensive Earthquake Catalog (black; M_{oth}), which are predominantly calculated using a duration-magnitude scale. Dots indicate all events within 250 km of the microseismic network; circles are for events within the project area.

Detection-Threshold Maps

Figure 22 shows the minimum-magnitude detection maps that were produced using the pseudo-theoretical approach described in the **Methods**

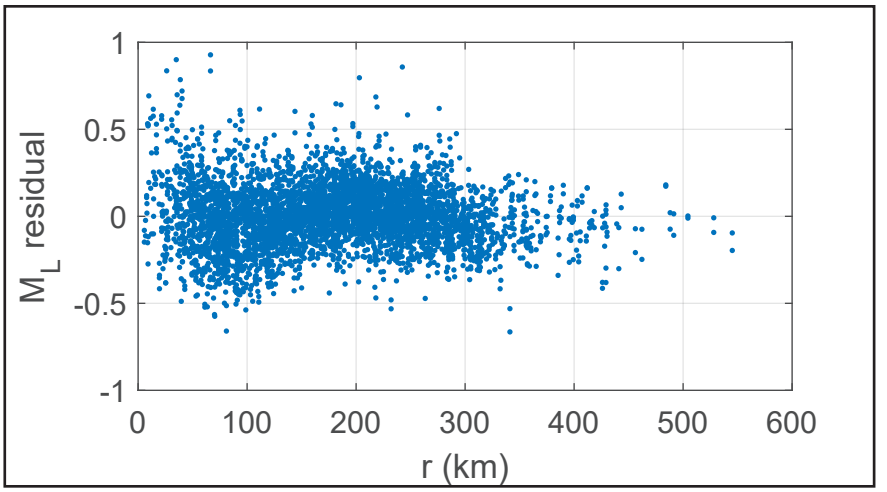

Figure 17. M_L residuals calculated as the event M_L minus the station M_L (using equation 3) versus hypocentral distance.

section. The maps represent the sensitivity of the fully operational monitoring network seismographic and contributing regional network stations, and do not account for telemetry or station outages. These maps indicate that minimum detectable magnitudes in the Rome Trough of eastern Kentucky in the vicinity of wastewater-disposal wells or deep oil and gas test wells range from M_w 0.5 in the southeast to M_w 0.7 for nighttime hours and from M_w 0.7 to 1.0 during daytime hours. Comparing the daytime ranges with those in the corresponding regions prior to the monitoring network's deployment (Fig. 6) demonstrates that the network improved the detection threshold for the region substantially: The previous minimum-magnitude ranges were M_w 1.5 to 1.9 and M_w 1.5 to 1.6, excluding and including the Central and Eastern United States Network stations, respectively.

Summary

The Rogersville Shale is a deep formation in the Rome Trough of eastern Kentucky that is being tested for oil and gas production. Because of the shale's low permeability, production requires unconventional methodologies—in particular, high-volume and high-pressure hydraulic fracturing. Because of the formation's proximity to the crystalline basement and its location within the faulted Rome Trough, however, there is a potential for inducing earthquakes when stimulating this shale. Also, the injection of produced wastewater for disposal, the chief culprit of inducing larger-magnitude (up to magnitude 5.8) earthquakes in places such as Oklahoma, Arkansas, and Ohio continues in the Rome Tough of eastern Kentucky.

To facilitate discrimination between potential induced earthquakes and natural seismicity, a network of sensitive seismic monitoring stations was installed in the Rome Trough of eastern Kentucky. This network improved the monitoring sensitivity in the vicinity of wastewater-injection wells and deep oil and gas wells testing the Rogersville Shale by approximately an entire unit of magnitude: With the Eastern Kentucky Microseismic Monitoring network, the detectable magnitudes range from 0.7 to 1.0 and without the network, the detectable magnitudes range from 1.5 to 1.9.

Using real-time recordings from this network in tandem with recordings of other temporary and permanent regional seismic stations, a catalog of local seismicity was developed. At the time this report was prepared, 151 earthquakes had been detected and located using the microseismic monitoring network's recordings, 38 of which were in the project area. Only six earthquakes occurred in the Rome Trough of eastern Kentucky, and none appear to be associated with the deep Rogersville Shale test wells that were completed during the time the network has been in operation, or in association with wastewater-injection wells. Furthermore, none of these six events were included in catalogs produced by other regional monitoring agencies.

As part of developing the seismicity catalog, a calibrated local-magnitude scale was developed for the monitoring project area. Using this scale and the event catalog from the period after all microseismic monitoring network stations were operating, the magnitude of completeness is estimated to be magnitude 1.4 in the project area. In other words, all events of magnitude 1.4 or greater within the project area are expected to have been detected by network stations used for this project. Modeling the detection threshold within the project area indicates that the theoretical detec-

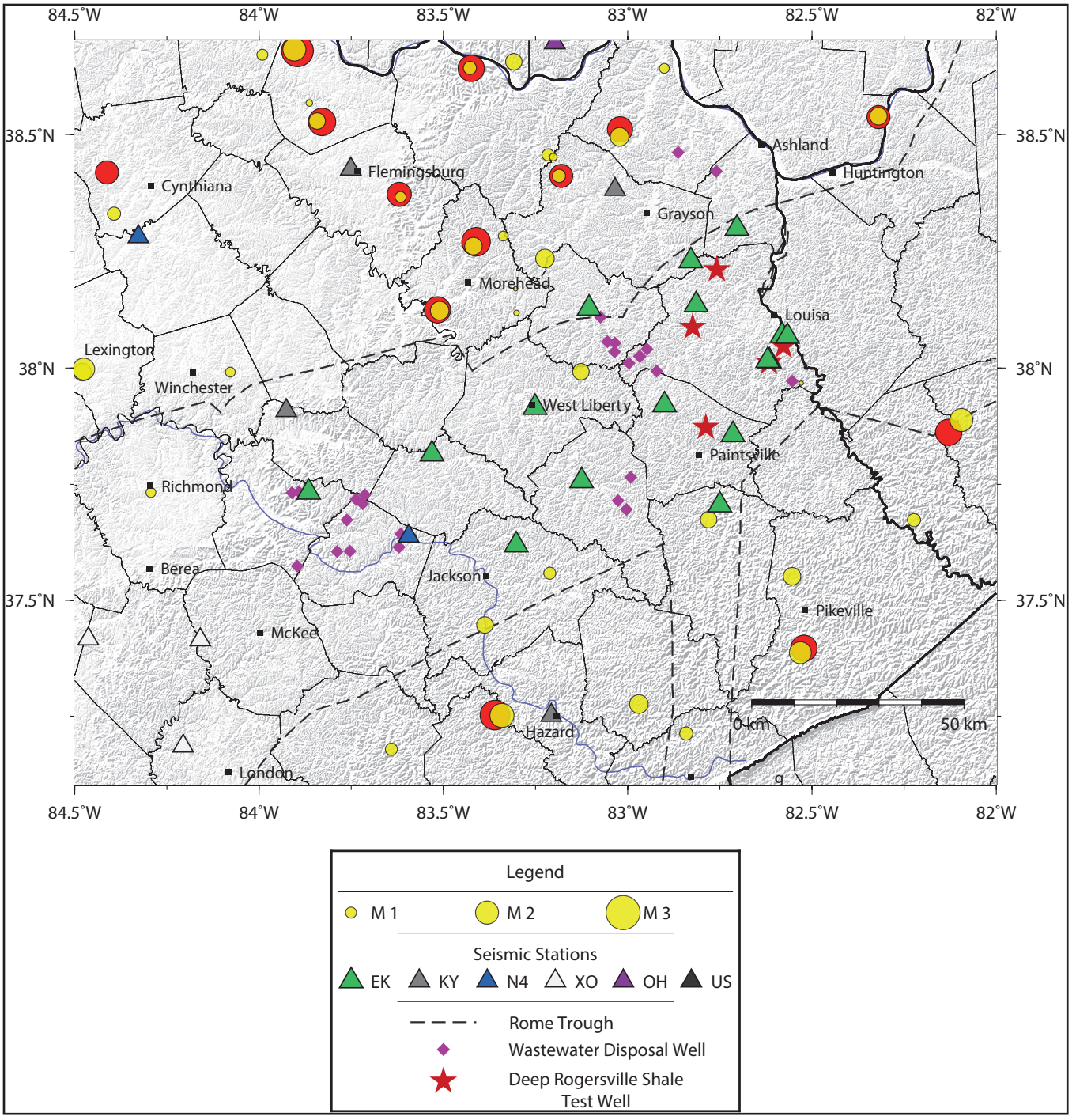

Figure 18. Seismicity located by the Eastern Kentucky Microseismic Monitoring Project (yellow) and in the Advanced National Seismic System Comprehensive Earthquake Catalog (red) for the same period.

tion threshold (minimum detectable magnitude) is as low as magnitude 0.5 in the project area, however. The discrepancy between the observed and modeled catalog completeness estimates is likely primarily of tectonic origin. Differences between daytime (greater noise levels) and nighttime (more seismically quiet) network sensitivity and occasional telemetry or station outages could have resulted in inconsistent detection of small events of magnitude approaching the detection threshold.

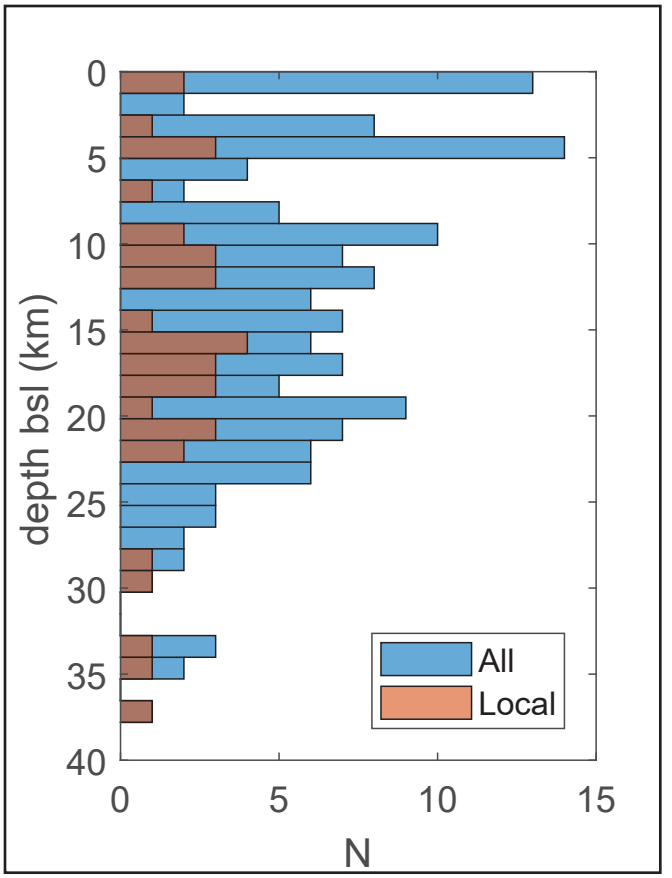

Figure 19. Depth distribution of earthquakes in the project area (red) and of all events recorded within 250 km of the Eastern Kentucky Microseismic Monitoring network (blue). Depths are with respect to sea level.

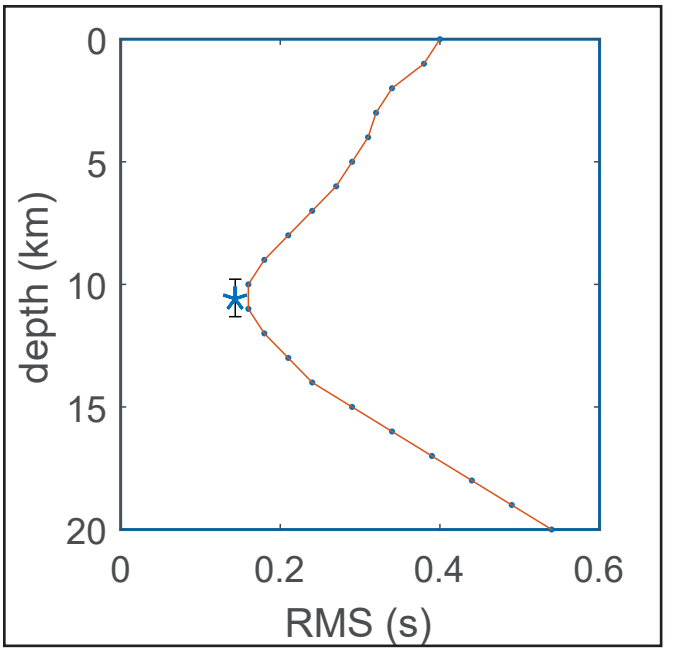

Figure 20. Focal depth versus root-mean-square traveltime misfit for the 02/20/2017 M_L 0.4 earthquake within 5 km of wastewater-injection well EPA ID KYS1270202. The best-fitting focal depth is indicated by the star; the formal error (uncertainty) in this depth determination is also shown by the vertical error bars.

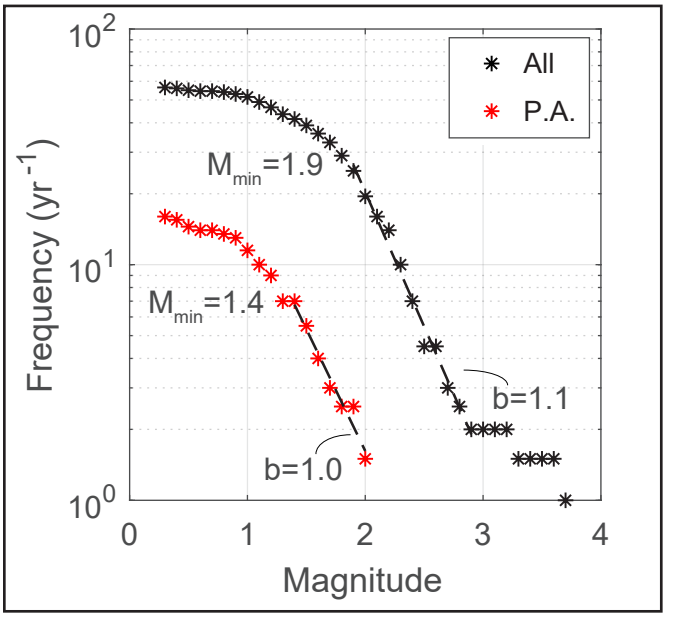

Figure 21. Gutenberg-Richter plots for located events in the project area (P.A.; red) and within 250 km of the Eastern Kentucky Microseismic Monitoring network stations (All; black) when the entire seismograph network was operational (June 2016–May 2018). The b-value, or negative slope on a semi-logarithmic scale, and the magnitude of completeness (M_{min}) are labeled on the best-fitting lines through the linear part of each plot.

Data and Resources

Eastern Kentucky Microseismic Monitoring Project recordings and metadata are available upon request; contact Seth Carpenter. Kentucky Seismic and Strong-Motion Network, operated jointly by the Kentucky Geological Survey and the University of Kentucky Department of Earth and Environmental Sciences, recordings are continuously archived at Incorporated Research Institutions for Seismology's Data Management Center (ds.iris.edu/ds/nodes/dmc; last accessed 02/21/2018) and at the Kentucky Geological Survey (doi:10.7914/SN/KY).

Acknowledgments

We wish to acknowledge the state of Kentucky for funding the majority of this study, including funding for the acquisition of new seismic instrumentation, without which the scope of the

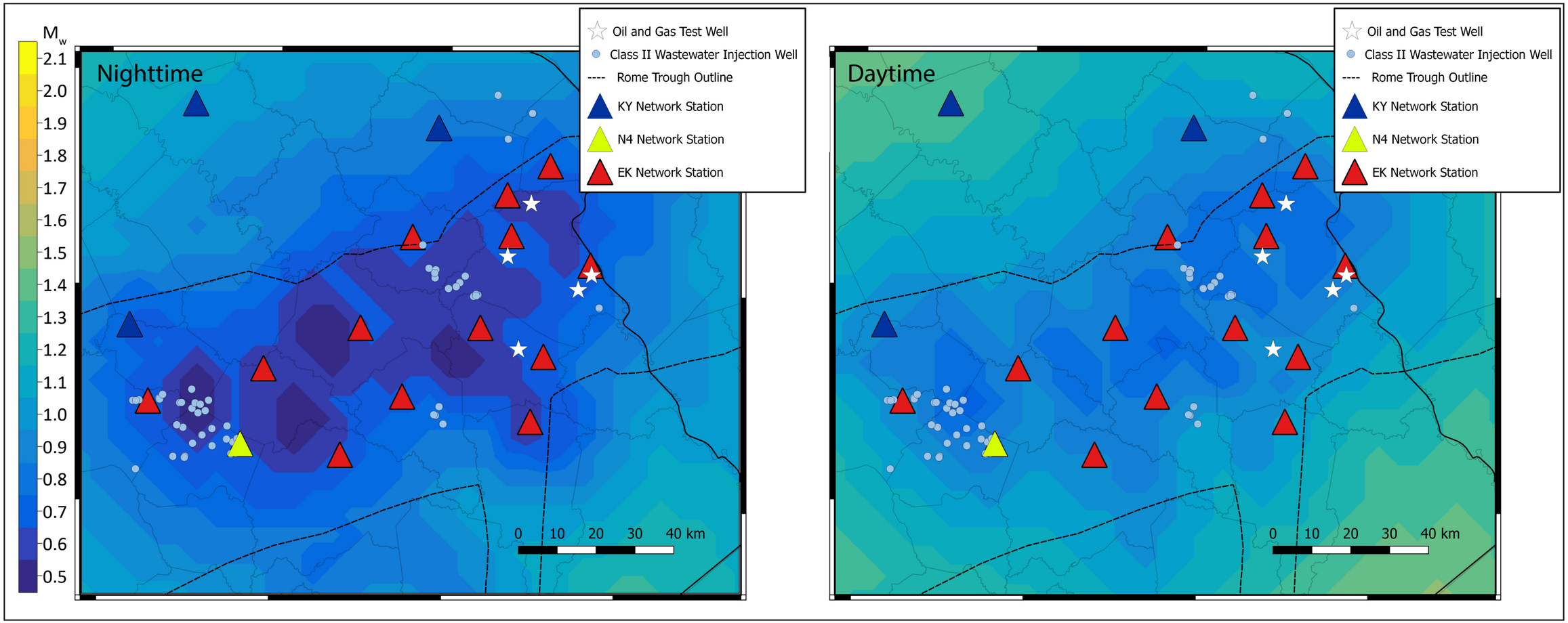

Figure 22. Nighttime (left) and daytime (right) minimum-magnitude detection thresholds in the project area. KY, N4, and EK are the network codes for the Kentucky Seismic and Strong-Motion, Central and Eastern United States Network (www.usarray.org/ceusn; last accessed 12/14/2018), and Eastern Kentucky Microseismic Monitoring Project networks, respectively.

study would have been severely reduced, and former KGS Associate Director Jerry Weisenfluh, who permitted and encouraged us to undertake this investigation. We also thank Cimarex Energy Co. for their generous loan of six complete seismograph stations for the duration of this project, Nanometrics for the contribution of one complete seismic station, and the University of Kentucky Department of Earth and Environmental Sciences for their financial assistance. We are grateful to Pioneer Natural Resources for funding Andrew Holcomb's research assistantship while he was a student in the Department of Earth and Environmental Sciences. We also thank Steven L. Roche for his input during this project. We are grateful to David Harris at KGS, who secured the partnership with Cimarex Energy Co., and helped us keep abreast of ongoing oil and gas activity in the Rogersville Shale. A key contribution to this project came from the landowners who offered locations for operation of the network stations. We appreciate the guidance and data sets from Tom Sparks at KGS, who helped us compile the table of Class II wastewater-disposal wells. We also greatly appreciate the support of Kati Ellis at KGS for purchasing and logistics and Mike Ellis for IT support. And we appreciate the help from the staff, researchers, students, and visiting scholars at UK who assisted with field work: Mike Lynch, Scott Waninger, Max Hammond, Matt Crawford, Jifeng Chen, Lifang Zhang, Junjie Sun, Jianhong Kang, and Paul Rodriguez-Asihama.

References Cited

Alsaker, A., Kvamme, L.B., Hansen, R.A., Dahle, A., and Bungum, H., 1991, The M_L scale in Norway: Bulletin of the Seismological Society of America, v. 81, no. 2, p. 379–398.

Atkinson, G.M., and Boore, D.M., 2014, The attenuation of Fourier amplitudes for rock sites in eastern North America: Bulletin of the Seismological Society of America, v. 104, no. 1, p. 513–528, doi:10.1785/0120130136.

Bao, X., and Eaton, D.W., 2016, Fault activation by hydraulic fracturing in western Canada: Science, v. 354, issue 6318, p. 1406–1409, doi:10.1126/science.aag2583.

Boatwright, J., 1980, A spectral theory for circular seismic sources; simple estimates of source dimension, dynamic stress drop, and radiated seismic energy: Bulletin of the Seismological Society of America, v. 70, no. 1, p. 1–27.

Bockholt, B.M., Langston, C.A., and Withers, M., 2015, Local magnitude and anomalous amplitude distance decay in the Eastern Tennessee Seismic Zone: Seismological Research Letters, v. 86, no. 33, p. 1040–1050, doi:10.1785/0220140201.

Burger, R.W., Somerville, P.G., Barker, J.S., Herrmann, R.B., and Helmberger, D.V., 1987, The effect of crustal structure on strong ground motion attenuation relations in eastern North America: Bulletin of the Seismological Society of America, v. 77, no. 2, p. 420–439.

Carpenter, N.S., Woolery, E.W., and Wang, Z., 2014, The M_w 4.2 Perry County, Kentucky, earthquake of 10 November 2012: Evidence of the Eastern Tennessee Seismic Zone in southeastern Kentucky: Seismological Research Letters, v. 85, no. 4, p. 931–939, doi:10.1785/0220130221.

Chapman, M.C., Mathena, E.C., and Snoke, J.A., 2002, Southeastern United States Seismic Network Bulletin: U.S. Geological Survey, Bulletin 36, www.magma.geos.vt.edu/vtso/anonftp/catalog/bul36.pdf [accessed 01/03/2018].

Chapman, M.C., Powell, C.A., Vlahovic, G., and Sibol, M.S., 1997, A statistical analysis of earthquake focal mechanisms and epicenter locations in the Eastern Tennessee Seismic Zone: Bulletin of the Seismological Society of America, v. 87, no. 6, p. 1522–1536.

Ellsworth, W.L., 2013, Injection-induced earthquakes: Science, v. 341, no. 6142, 1225942, doi:10.1126/science.1225942.

Gao, D., Shumaker, R.C., and Wilson, T.H., 2000, Along-axis segmentation and growth history of the Rome Trough in the central Appalachian Basin: American Association of Petroleum Geologists Bulletin, v. 84, no. 1, p. 75–99.

Harris, D.C., 2015, Cambrian Rogersville Shale in the Rome Trough, Kentucky and West Virginia: A potential new unconventional reservoir in the Appalachian Basin: American Association of Petroleum Geologists Search and Discovery Article 10787, www.searchanddiscovery.com/pdfz/documents/2015/10764hickman/ndx_hickman.pdf.html [accessed 12/10/2018].

Harris, D.C., Drahovzal, J.A., Hickman, J.B., Nuttall, B.C., Baranoski, M.T., and Avary, K.L., 2004, Rome Trough Consortium final report and data distribution: Kentucky Geological Survey, ser. 12, Open-File Report OF-04-06, 1 CD-ROM.

Havskov, J., and Ottemöller, L., 1999, SEISAN earthquake analysis software: Seismological Research Letters, v. 70, no. 5, p. 532–534.

Heidbach, O., Tingay, M., Barth, A., Reinecker, J., Kurfeß, D., and Müller, B., 2008, The world stress map database release 2008: dc-app3-14.gfz-potsdam.de/pub/stress_maps/stress_maps.html [accessed 12/14/2018].

Herrmann, R.B., 1983, Short-period Lg magnitudes: Instrument, attenuation, and source effects: Bulletin of the Seismological Society of America, v. 73, no. 6A, p. 1835–1850.

Herrmann, R.B., and Ammon, C.J., 1997, Faulting parameters of earthquakes in the New Madrid, Missouri, region: Engineering Geology, v. 46, nos. 3-4, p. 299–311.

Herrmann, R.B., Langston, C.A., and Zollweg, J.E., 1982, The Sharpsburg, Kentucky, earthquake of 27 July 1980: Bulletin of the Seismological Society of America, v. 72, no. 4, p. 1219–1239.

Hickman, J.B., 2011, Structural evolution of an intracratonic rift system; Mississippi Valley Graben, Rough Creek Graben, and Rome Trough of Kentucky, USA: Lexington, University of Kentucky, doctoral dissertation, 186 p., 31 plates.

Hickman, J.B., Harris, D.C., and Eble, C.F., 2015, Cambrian Rogersville Shale in the Rome Trough, Kentucky and West Virginia: A potential new unconventional reservoir in the Appalachian Basin: American Association of Petroleum Geologists Search and Discovery Article 2103714, www.searchanddiscovery.com/abstracts/html/2015/90216ace/abstracts/2103714.html [accessed 12/10/2018].

Holcomb, A., 2017, Initial microseismic recordings at the onset of unconventional hydrocarbon development in the Rome Trough, eastern Kentucky: Lexington, University of Kentucky, master's thesis, 225 p., doi.org/10.13023/ETD.2017.316.

Holland, A.A., 2013, Earthquakes triggered by hydraulic fracturing in south-central Oklahoma: Bulletin of the Seismological Society of America, v. 103, no. 3, p. 1784–1792, doi:10.1785/0120120109.

Hornbach, M.J., DeShon, H.R., Ellsworth, W.L., Stump, B.W., Hayward, C., Frohlich, C., Oldham, H.R., Olson, J.E., Magnani, M.B., Brokaw, C., and Luetgert, J.H., 2015, Causal factors for seismicity near Azle, Texas: Nature Communications, v. 6, article 6728, www.nature.com/articles/ncomms7728 [accessed 12/10/2018].

Horton, S., 2012, Disposal of hydrofracking waste fluid by injection into subsurface aquifers triggers earthquake swarm in central Arkansas with potential for damaging earthquake: Seismological Research Letters, v. 83, no. 2, p. 250–260, doi.org/10.1785/gssrl.83.2.250.

Hutton, L.K., and Boore, D.M., 1987, The M_L scale in southern California: Bulletin of the Seismological Society of America, v. 77, no. 6, p. 2074–2094.

Johnson, C.E., Bittenbinder, A., Bogaert, B., Dietz, L., and Kohler, W., 1995, Earthworm: A flexible approach to seismic network processing: IRIS Newsletter, v. 14, no. 2, p. 1–4.

Kentucky Geological Survey, 2014, Induced seismic events in Kentucky: Kentucky Geological Survey, Fact Sheet, 4 p., www.uky.edu/KGS/education/factsheet-InducedSeismicEvents.pdf [accessed 12/10/2018].

Keranen, K.M., Savage, H.M., Abers, G.A., and Cochran, E.S., 2013, Potentially induced earthquakes in Oklahoma, USA: Links between wastewater injection and the 2011 M_w 5.7 earthquake sequence: Geology, v. 41, no. 6, p. 699–702, doi.org/10.1130/G34045.1.

Kim, W.Y., 1998, The M_L scale in eastern North America: Bulletin of the Seismological Society of America, v. 88, no. 4, p. 935–951.

Langenbruch, C., and Zoback, M.D., 2016, How will induced seismicity in Oklahoma respond to decreased saltwater injection rates?: Science Advances, v. 2, no. 11, e1601542, doi:10.1126/sciadv.1601542.

Lienert, B.R., and Havskov, J., 1995, A computer program for locating earthquakes both locally and globally: Seismological Research Letters, v. 66, no. 5, p. 26–36.

McNamara, D.E., and Boaz, R.I., 2011, PQLX: A seismic data quality control system description, applications, and users manual: U.S. Geological Survey Open-File Report 2010-1292, 41 p.

National Research Council, 2013, Induced seismicity potential in energy technologies: Washington, D.C., The National Academies Press, 262 p., doi.org/10.17226/13355.

Richter, C.F., 1935, An instrumental earthquake magnitude scale: Bulletin of the Seismological Society of America, v. 28, no. 1, p. 1–32.

Rubinstein, J.L., Ellsworth, W.L., McGarr, A., and Benz, H.M., 2014, The 2001–present induced earthquake sequence in the Raton Basin of northern New Mexico and southern Colorado: Bulletin of the Seismological Society of America, v. 104, no. 5, p. 2162–2181, doi:10.1785/0120140009.

Skoumal, R.J., Brudzinski, M.R., and Currie, B.S., 2015, Earthquakes induced by hydraulic fracturing in Poland Township, Ohio: Bulletin of the Seismological Society of America, v. 105, no. 1, p. 189–197, doi:10.1785/0120140168.

Sloss, L.L., 1988, Tectonic evolution of the craton in Phanerozoic time, *in* Sloss, L.L., ed., Sedimentary cover—North American craton: Geological Society of America, DNAG, Geology of North America, v. D-2, p. 25–51.

Sparks, T.N., 2016, Class II injection wells in Kentucky—An update of the map service of wastewater, brine-disposal, and enhanced-recovery wells in Kentucky [abs.]: American Association of Petroleum Geologists–Eastern Section 45th annual meeting, Program with Abstracts, p. 58.

Sparks, T.N., and Curl, D.C., 2014, Class I and Class II wells in Kentucky (disposal and injection wells): Kentucky Geological Survey, kygs.maps.arcgis.com/home/webmap/viewer.html?webmap=9380ec4940cd46c9b2c65a1160753f6f [accessed 12/10/2018].

Stein, S., and Wysession, M., 2009, An introduction to seismology, earthquakes, and earth structure: New York, Wiley, 499 p.

Taylor, J., Celebi, M., Greer, A., Jampole, E., Masroor, A., Melton, S., Norton, D., Paul, N., Wilson, E., and Xiao, Y., 2017, EERI Earthquake Reconnaissance Team Report: M5.0 Cushing, Oklahoma, USA earthquake on November 7, 2016: EERI Learning From Earthquakes Program, 25 p., www.researchgate.net/publication/320357434_EERI_Earthquake_Reconnaissance_Team_Report_M50_Cushing_Oklahoma_USA_Earthquake_on_November_7_2016 [accessed 12/10/2018].

Weingarten, M., Ge, S., Godt, J.W., Bekins, B.A., and Rubinstein, J.L., 2015, High-rate injection is associated with the increase in US Mid-continent seismicity: Science, v. 348, no. 6241, p. 1336–1340, doi:10.1126/science.aab1345.

Wiemer, S., and Wyss, M., 2000, Minimum magnitude of completeness in earthquake catalogs: Examples from Alaska, the western United States, and Japan: Bulletin of the Seismological Society of America, v. 90, no. 4, p. 859–869.

White, T.M., 2001, Fault kinematics of the Rome Trough [abs.]: Geological Society of America Abstracts with Programs, v. 33, no. 4, p. 42.

Withers, M., Aster, R., Young, C., Beiriger, J., Harris, M., Moore, S., and Trujillo, J., 1998, A comparison of select trigger algorithms for automated global seismic phase and event detection: Bulletin of the Seismological Society of America, v. 88, no. 1, p. 95–106.

Yang, X., Pavlis, G.L., Hamburger, M.W., Sherrill, E., Gilbert, H., Marshak, S., Rupp, J., and Larson, T.H., 2014, Seismicity of the Ste. Genevieve Seismic Zone based on observations from the EarthScope OIINK flexible array: Seismological Research Letters, v. 85, no. 6, p. 1285–1294, doi:10.1785/0220140079.

Yeck, W.L., Hayes, G.P., McNamara, D.E., Rubinstein, J.L., Barnhart, W.D., Earle, P.S., and Benz, H.M., 2017, Oklahoma experiences largest earthquake during ongoing regional wastewater injection hazard mitigation efforts: Geophysical Research Letters, v. 44, no. 2, p. 711–717, doi.org/10.1002/2016GL071685.

Zoback, M.D., Townend, J., and Grollimund, B., 2002, Steady-state failure equilibrium and deformation of intraplate lithosphere: International Geology Review, v. 44, no. 5, p. 383–401.

Zoback, M.L., and Zoback, M.D., 1989, Tectonic stress field of the continental United States: Geophysical framework of the continental United States: Geological Society of America Memoir, v. 172, p. 523–539.